CONTROLLED SOURCE ELECTROMAGNETIC DEEP SOUNDING: THEORY, RESULTS AND CORRELATION WITH NATURAL SOURCE RESULTS

DAVID E. BOERNER

Continental Geoscience Division, Geological Survey of Canada, 1 Observatory Crescent, Ottawa, Ontario, Canada K1A 0Y3

(Received 27 November 1990; accepted 21 June 1991)

Abstract. Controlled source electromagnetic (EM) methods represent a unique set of geophysical experiments which can be used to determine the properties and state of the deep continental crust. Unlike natural source EM methods, an artificial EM source technique can be designed to optimize resolution and minimize interactions with local structure. The major drawbacks include restricted depth penetration, insufficient data sets and a limited number of modelling algorithms. Information about the electrical conductivity at lower crustal depths can be obtained but at the expense of requiring large moment sources, sophisticated processing techniques and data redundancy. Moreover, EM data are sufficiently complicated that numerical modelling is often necessary for quantitative interpretation. It is therefore essential to record enough information to justify the choice of interpretation algorithms, particularly since controlled source EM forward modelling routines are generally very restrictive and not widely available. As most interpretations are based on layered earth models, observations of all the EM field components can be useful for testing the "dimensionality" of the data and for justifying interpretations.

1. Introduction

Electromagnetic (EM) sounding methods represent one of the few geoscientific techniques which can provide information about the current state and properties of the deep continental crust and upper mantle. EM soundings respond to the distribution of electrical conductivity which is the most highly variable physical property of rocks and minerals. Conductivity is controlled by paths of ionic conduction (determined, for example, by porosity, pore fluid salinity and saturation, and by the presence of partial melt) or paths of electronic conduction (e.g. metallic minerals, carbon on grain boundaries). Consequently, EM techniques represent an exciting and challenging class of experiments with which to examine the structure, state and composition of the crust and upper mantle.

The EM methods which have been traditionally applied for sounding the deep crust use the temporal variations of the natural fields to image the conductivity structure of the earth. The principle reason for this is that natural fields are essentially plane waves in the mid-latitudes and have sufficient energy at long periods to generate a detectable response from very deep structure. However, the use of natural source fields has at once benefits as well as problems. There are low energy regions in the natural source frequency spectrum and the signal levels

Surveys in Geophysics **13**: 435–488, 1992.

can change dramatically over a relatively short time span making data acquisition demanding and time consuming. As well, the large spatial extent of the plane wave fields produces response in the data from structures at some horizontal distance from the receiver location. Such lateral responses, when coupled with uncertainties about both the source field characteristics and geology, complicate the already difficult task of data interpretation.

Controlled source EM (CSEM) methods are an attractive compliment or alternative to natural source soundings in some circumstances. In these experiments the source characteristics are precisely known and can be located to configure the excitation fields in an optimal geometrical form. Furthermore, the source frequency spectrum can be tailored for the particular experiment. One important limitation of CSEM is that the source moment is small relative to that of natural sources, and this effectively limits the penetration of the EM fields at low frequency. Another complication is that CSEM fields are substantially more difficult to model than plane wave fields and thus care must be taken to avoid experimental configurations and geological environments in which the EM response is not interpretable. With these concerns in mind, it is hardly surprising that CSEM methods are not common in deep sounding experiments where little geological or geophysical control is available as auxiliary information. There are, however, several good examples of deep CSEM probing of the crust which have produced reliable and useful results.

The CSEM literature is extensive and much of the work on shallow (i.e. <2 km) sounding can be scaled so as to be relevant for crustal investigations. Spies and Frischknecht (1991) discuss electromagnetic sounding in detail and give important information about the commercial and private EM systems currently in use. A recent, general overview of CSEM sounding in sedimentary structures was presented by Nekut and Spies (1989) who discuss several aspects of theory and current interpretation methods. Nagy (1988) compared fourteen different classes of CSEM methods and also reviewed some of the basic literature for each technique. In addition, there are several monographs which provide insightful and complete descriptions of CSEM methods (e.g., Vanyan, 1965; Wait, 1982; Kaufman and Keller, 1983; Ward and Hohmann, 1988).

There have also been excellent reviews which specifically address different aspects of deep CSEM sounding. Ward (1983) discussed the specifications required for crustal EM sounding including consideration of natural and cultural noise, resolution, current channelling and depth of exploration. Ward (1983) also showed the deleterious affects of performing the sounding in the vicinity of near surface structure when the EM response of the structure is not accounted for. Many theoretical and practical difficulties encountered in deep sounding are dealt with by Kaufman and Keller (1983) who also provide some interesting examples (mainly geothermal) of deep sounding. The EM induction reviews (primarily for North

America) by Hermance (1983) and Chave and Booker (1987) give an overview of the role CSEM techniques have played in deep sounding programs.

This paper is intended as a general review of controlled source theory, methods and applications to deep sounding problems. Because there are a plethora of possible variations on basic EM sounding techniques the review begins with an introduction of the mathematical and physical characteristics of EM source fields necessary for understanding the different experiments. It is only with an appreciation of the theory describing EM sources that the similarities, capabilities and limitations of the different deep sounding CSEM techniques can be judged. With this background as a reference, the results of several important deep sounding experiments are used to illustrate certain aspects of CSEM.

In an effort to conserve space, many logistical and experimental design considerations for optimal CSEM deep sounding will not be discussed. However, such practical aspects may be more important to the overall success of a survey than theoretical forward modelling, inversion and sensitivity studies. One good example is the choice of a transmitter waveform which, when coupled with the receiver response, may govern

- the maximum depth of investigation (Spies, 1989),
- the minimum dynamic range required of a receiver system (e.g. West *et al.*, 1984),
- the necessity and difficulty of source response deconvolution (e.g. Asten, 1987, Strack *et al.*, 1989a),
- the minimum power requirements of the transmitter (e.g. Duncan *et al.*, 1980) and
- the accuracy of the receiver calibration (Sternberg, 1990),

as well as signal to noise ratios, signal bandwidth, etc. The literature describing CSEM methods can be somewhat biased towards theory since the trade-offs made during instrumental and experimental design are rarely discussed in much detail. However, efforts devoted to addressing the practical difficulties of deep EM sounding which may alleviate subsequent problems or limitations with data interpretation are certainly desirable.

Another important aspect of CSEM which will not be discussed in detail here is the deficiency of suitable modelling and interpretational aids. Without adequate modelling, experimental design becomes an exercise in intuition and extrapolation from 1D responses. The subsequent interpretation is also incomplete, and possibly unreliable. Most of the deep controlled source work published in the literature reflects the difficulties of multi-dimensional modelling in that the resulting interpretations are usually based on 1D earth responses. There are some notable exceptions to this trend (e.g. Sternberg and Clay, 1977; Kaikkonen *et al.*, 1988; Vanyan *et al.*, 1989), although even these interpretations are based on models of special

cases. The current capabilities for physical or numerical modelling of complicated media must be expanded if CSEM methods are to be used in complicated geological environments and achieve more of the promise that they hold.

Finally, no attempt will be made to discuss the physical or geological significance of deep conductivity structure. Such problems represent a complicated topic with an extensive literature base which could not be adequately covered in this review. The interested reader is referred to the individual papers about each sounding as a starting point for physical interpretations.

2. EM Dipole Sources in a 1D Earth

The theory describing the behavior of EM dipole sources is well known for one-dimensional conductivity models. There are several excellent descriptions of the derivation of EM fields from these sources starting from Maxwell's equations (e.g. Vanyan, 1965; Wait, 1982; Kaufman and Keller, 1983; Ward and Hohmann, 1988). While the real earth is not often one-dimensional, such models may be applicable in quasi-layered settings. 1D models excited by finite sources can provide a number of important insights into EM sounding and also serve as a basis for sensitivity studies and three-dimensional modelling. The purpose of this section is to review the mathematical description of the fields from dipole sources in a 1D earth in such a fashion that the physics underlying each possible source/receiver combination remains clear.

Any EM source can be represented by a spatial distribution of current composed of infinitesimally small electric dipoles. However, when solving Maxwell's equations it is often convenient to rely on the field duality condition and introduce symmetries in the equations through the concept of a magnetic dipole (representative of an infinitesimally small, divergenceless current flow). All electrical and EM prospecting methods are simply variations on this basic theme of electric and magnetic dipoles. As well, the duality between EM sources and the boundary conditions on conductivity structures implies that dipole sources play an integral part in describing the interaction of EM fields with complicated media.

Consider Maxwell's equations and a single Fourier component proportional to $e^{i\omega t}$,

$$\nabla \cdot \mathbf{B} = 0 \tag{1}$$

$$\nabla \times \mathbf{E} + i\omega\mathbf{B} = i\omega\mu\mathbf{J}'_m \tag{2}$$

$$\nabla \times \mathbf{B} - \mu\boldsymbol{\alpha}\mathbf{E} = \mu\mathbf{J}'_e. \tag{3}$$

$i = \sqrt{-1}$, ω is the angular frequency, $\mathbf{E}$ is the electric field, $\mathbf{B}$ is the magnetic

induction, while $\mathbf{J}'_e$ and $\mathbf{J}'_m$ are the applied electric and magnetic source currents, respectively. When the frequency of oscillation is low enough that the EM fields are diffusive (quasi-static), the impressed source currents can be assumed to be unaffected by **E** and **B**.

The electrical properties of the media are given by the magnetic permeability μ and the admittivity tensor, chosen here to represent a uniform and transversely isotropic earth,

$$\boldsymbol{\alpha} = \begin{bmatrix} \sigma_h + i\omega\epsilon_h & 0 & 0 \\ 0 & \sigma_h + i\omega\epsilon_h & 0 \\ 0 & 0 & \sigma_v + i\omega\epsilon_v \end{bmatrix} = \begin{bmatrix} \alpha_h & 0 & 0 \\ 0 & \alpha_h & 0 \\ 0 & 0 & \alpha_v \end{bmatrix}, \tag{4}$$

where σ is the electrical conductivity and ϵ is the permittivity. For the 1D development, the spatial variation of these parameters is confined to the vertical (z) direction where z is perpendicular to the layering.

Because of the assumed cylindrical symmetry of the admittivity tensor about the z-axis, it is possible to express the solution to Maxwell's equations in the Hankel domain (i.e. the radial Fourier domain). The behavior of the fields is determined by obtaining solutions to the Helmholtz equation in the Hankel domain and imposing the boundary conditions on these solutions at sources and at property contrasts. An inverse Hankel operator is then employed to transform the results to the space domain.

This rather standard approach to solving boundary value problems has an interesting aspect for 1D models in that all six EM field components from any source can be represented in terms of just two scalar potentials. The scalars can be conveniently chosen to represent two uncoupled modes of current flow which can be described geometrically as "toroidal" and "poloidal". That just two scalar potentials are sufficient to represent every combination of sources and receivers in a layered earth is an indication of the redundancy between different electrical and EM methods.

Instead of presenting the details of the layered earth response to EM excitation (which appear in many other places), it is perhaps more useful simply to identify some of the key results necessary for understanding the data and assessing the interpretations of different CSEM experiments. The basis for this discussion is a generalized solution of the Helmholtz equation (Boerner and West, 1989a) for both electric and magnetic dipole sources in a layered earth. The EM fields of a dipole source can be written as the Hankel transform of a generic source matrix $\tilde{\mathscr{F}}$ and a set of spatial operators,

$$\begin{bmatrix} E_x \\ E_y \\ E_z \\ B_x \\ B_y \\ B_z \end{bmatrix} = \frac{1}{4\pi} \int_0^\infty \tilde{\mathscr{F}} \begin{bmatrix} \partial_{xx} \\ \partial_{xy} \\ \partial_x \\ \partial_y \\ 1 \end{bmatrix} \lambda J_0(\lambda\xi)\, d\lambda. \tag{5}$$

Here $\xi = \sqrt{r^2 + r'^2 - 2rr' \cos(\phi - \phi')}$ is the translationally and rotationally invariant radial distance between the source point (r', ϕ', z') and receiver point (r, ϕ, z) while λ is the horizontal (radial) wavenumber. Equation (5) was derived with the specific intent of isolating the geometrical variations of the fields (i.e., the spatial derivatives) from the electromagnetic interactions with the layered earth. Consider the fields of spatially extended sources which are found by the integration of Equation (5) over the dimensions of the source. The spatial derivatives, the integration over the source volume and the transformation to the space domain can be identified as "geometrical operators" which are invariant with respect to changes in the layered earth model. As a result, when comparing and contrasting the capabilities of different EM source/receiver combinations many of the complicating factors are purely geometrical and thus independent of the earth model (i.e., the generic source matrix $\tilde{\mathscr{F}}$).

One key piece of information for comparing various methods is contained in the modal potentials of the source matrices. The source matrices for magnetic and electric dipoles are given in Table I in terms of toroidal magnetic (TM) and poloidal magnetic (PM) field modes (the symbols T_n and P_n respectively). The rows of each source matrix correspond to an EM field component (E_x, E_y, E_z, B_x, B_y, B_z), while the columns relate to the spatial behavior of the component. A toroidal magnetic field is associated with a poloidal current flow which, by virtue of crossing conductivity gradients in a layered earth, is sensitive to charge distributions. Conversely, a poloidal magnetic field is characterized by horizontal toroidal currents and is sensitive to the absolute value of the horizontal conductivity.

A schematic representation of the two uncoupled modes is shown in Figure 1. This parametric surface plot is constructed from the two sets of lines which represent the geometrical configuration of the poloidal and toroidal modes (in the region $x \leq 0$). Figure 1 may be reminiscent of several different images of EM current flow patterns such as the apparent smoke rings from loop source transient EM systems (e.g. Nabighian, 1979), or the current flow pattern around a grounded bipole. However, the modes are only pure representations of the current flow from EM sources in a uniform whole space. Although separable in a 1D earth, both modes are generally required to represent the current flow created by an arbitrary EM source or conductivity structure.

TABLE I

Source matrix definitions for the generalized representation of EM dipole fields. The TM and PM modes can be distinguished by the variables T_n and P_n, respectively, λ is the horizontal wavenumber, μ is the magnetic permeability. The vertical wavenumbers are $u = (\lambda^2 + i\omega\mu\alpha_h)^{1/2}$, $v = (K^2\lambda^2 + i\omega\mu\alpha_h)^{1/2}$, where $K^2 = \alpha_h/\alpha_v$ is the coefficient of anisotropy, and the subscripts S and R refer to parameters describing the media containing the source or receiver, respectively (see Boerner and West, 1989a for a complete description of the variables used in this table).

$\mathcal{F}_e = \mathrm{d}l$

$$\begin{bmatrix}
\frac{1}{\lambda^2}\left(\frac{\nu_R}{K_R^2}\frac{\tilde{T}_3}{\alpha_{v,S}} - i\omega\mu_R\frac{\tilde{P}_1}{u_S}\right)I'_{x,e} & \frac{1}{\lambda^2}\left(\frac{\nu_R}{K_R^2}\frac{\tilde{T}_3}{\alpha_{v,S}} - i\omega\mu_R\frac{\tilde{P}_1}{u_S}\right)I'_{y,e} & -\frac{\nu_R}{\nu_S}\frac{K_S^2}{K_R^2}\frac{\tilde{T}_2}{\alpha_{v,S}}I'_{z,e} & 0 & -i\omega\mu_R\frac{\tilde{P}_1}{u_S}I'_{x,e} \\
\frac{1}{\lambda^2}\left(i\omega\mu_R\frac{\tilde{P}_1}{u_S} - \frac{\nu_R}{K_R^2}\frac{\tilde{T}_3}{\alpha_{v,S}}\right)I'_{y,e} & \frac{1}{\lambda^2}\left(\frac{\nu_R}{K_R^2}\frac{\tilde{T}_3}{\alpha_{v,S}} - i\omega\mu_R\frac{\tilde{P}_1}{u_S}\right)I'_{x,e} & 0 & -\frac{\nu_R}{\nu_S}\frac{K_S^2}{K_R^2}\frac{\tilde{T}_2}{\alpha_{v,S}}I'_{z,e} & -\frac{\nu_R}{K_R^2}\frac{\tilde{T}_3}{\alpha_{v,S}}I'_{y,e} \\
0 & 0 & -\frac{\tilde{T}_4}{\alpha_{v,S}}I'_{x,e} & -\frac{\tilde{T}_4}{\alpha_{v,S}}I'_{y,e} & \lambda^2\frac{K_S^2\tilde{T}_1}{\nu_S\alpha_{v,S}}I'_{z,e} \\
\frac{\mu_R}{\lambda^2}\left(\mu_R\frac{\alpha_{v,R}}{\alpha_{v,S}}\tilde{T}_4 - \mu_R\frac{u_R}{u_S}\tilde{P}_2\right)I'_{y,e} & \frac{\mu_R}{\lambda^2}\left(\mu_R\frac{u_R}{u_S}\tilde{P}_2 - \mu_R\frac{\alpha_{v,R}}{\alpha_{v,S}}\tilde{T}_4\right)I'_{x,e} & 0 & \mu_R\frac{\alpha_{v,R}}{\alpha_{v,S}}\frac{K_S^2\tilde{T}_1}{\nu_S}I'_{z,e} & \mu_R\frac{\alpha_{v,R}}{\alpha_{v,S}}\tilde{T}_4I'_{y,e} \\
\frac{\mu_R}{\lambda^2}\left(\mu_R\frac{\alpha_{v,R}}{\alpha_{v,S}}\tilde{T}_4 - \mu_R\frac{u_R}{u_S}\tilde{P}_2\right)I'_{x,e} & \frac{\mu_R}{\lambda^2}\left(\mu_R\frac{\alpha_{v,R}}{\alpha_{v,S}}\tilde{T}_4 - \mu_R\frac{u_R}{u_S}\tilde{P}_2\right)I'_{y,e} & -\mu_R\frac{\alpha_{v,R}}{\alpha_{v,S}}\frac{K_S^2\tilde{T}_1}{\nu_S}I'_{z,e} & 0 & -\mu_R\frac{\mu_R}{u_S}\tilde{P}_2I'_{x,e} \\
0 & 0 & \mu_R\frac{\tilde{P}_1}{u_S}I'_{y,e} & -\mu_R\frac{\tilde{P}_1}{u_S}I'_{x,e} & 0
\end{bmatrix}$$

$\mathcal{F}_m = i\omega\mu_S\,\mathrm{d}A$

$$\begin{bmatrix}
\frac{1}{\lambda^2}\left(\frac{K_S^2}{K_R^2}\frac{\nu_R}{\nu_S}\tilde{T}_2 - \frac{\mu_R}{\mu_S}\tilde{P}_4\right)I'_{y,m} & \frac{1}{\lambda^2}\left(\frac{\mu_R}{\mu_S}\tilde{P}_4 - \frac{K_S^2}{K_R^2}\frac{\nu_R}{\nu_S}\tilde{T}_2\right)I'_{x,m} & 0 & -\frac{\mu_R}{\mu_S}\frac{\tilde{P}_1}{u_S}I'_{z,m} & -\frac{\mu_R}{\mu_S}\tilde{P}_4I'_{y,m} \\
\frac{1}{\lambda^2}\left(\frac{K_S^2}{K_R^2}\frac{\nu_R}{\nu_S}\tilde{T}_2 - \frac{\mu_R}{\mu_S}\tilde{P}_4\right)I'_{x,m} & \frac{1}{\lambda^2}\left(\frac{K_S^2}{K_R^2}\frac{\nu_R}{\nu_S}\tilde{T}_2 - \frac{\mu_R}{\mu_S}\tilde{P}_4\right)I'_{y,m} & \frac{\mu_R}{\mu_S}\frac{\tilde{P}_1}{u_S}I'_{z,m} & 0 & \frac{K_S^2}{K_R^2}\frac{\nu_R}{\nu_S}\tilde{T}_2I'_{x,m} \\
0 & 0 & -\frac{K_S^2\tilde{T}_1}{\nu_S}I'_{y,m} & \frac{K_S^2\tilde{T}_1}{\nu_S}I'_{x,m} & 0 \\
\frac{\mu_R}{\lambda^2}\left(\alpha_{v,R}\frac{K_S^2\tilde{T}_1}{\nu_S} - \frac{u_R\tilde{P}_3}{i\omega\mu_S}\right)I'_{x,m} & \frac{\mu_R}{\lambda^2}\left(\alpha_{v,R}\frac{K_S^2\tilde{T}_1}{\nu_S} - \frac{u_R\tilde{P}_3}{i\omega\mu_S}\right)I'_{y,m} & \frac{\mu_R}{\mu_S}\frac{u_R}{u_S}\frac{\tilde{P}_2}{i\omega}I'_{z,m} & 0 & \mu_R\alpha_{v,R}\frac{K_S^2\tilde{T}_1}{\nu_S}I'_{x,m} \\
\frac{\mu_R}{\lambda^2}\left(\frac{u_R\tilde{P}_3}{i\omega\mu_S} - \alpha_{v,R}\frac{K_S^2\tilde{T}_1}{\nu_S}\right)I'_{y,m} & \frac{\mu_R}{\lambda^2}\left(\alpha_{v,R}\frac{K_S^2\tilde{T}_1}{\nu_S} - \frac{u_R\tilde{P}_3}{i\omega\mu_S}\right)I'_{x,m} & 0 & \frac{\mu_R}{\mu_S}\frac{u_R}{u_S}\frac{\tilde{P}_2}{i\omega}I'_{z,m} & \frac{\mu_R}{\mu_S}\frac{u_R\tilde{P}_3}{i\omega}I'_{y,m} \\
0 & 0 & -\frac{\mu_R}{\mu_S}\frac{\tilde{P}_4}{i\omega}I'_{x,m} & -\frac{\mu_R}{\mu_S}\frac{\tilde{P}_4}{i\omega}I'_{y,m} & \lambda^2\frac{\mu_R}{\mu_S}\frac{\tilde{P}_1}{i\omega u_S}I'_{z,m}
\end{bmatrix}$$

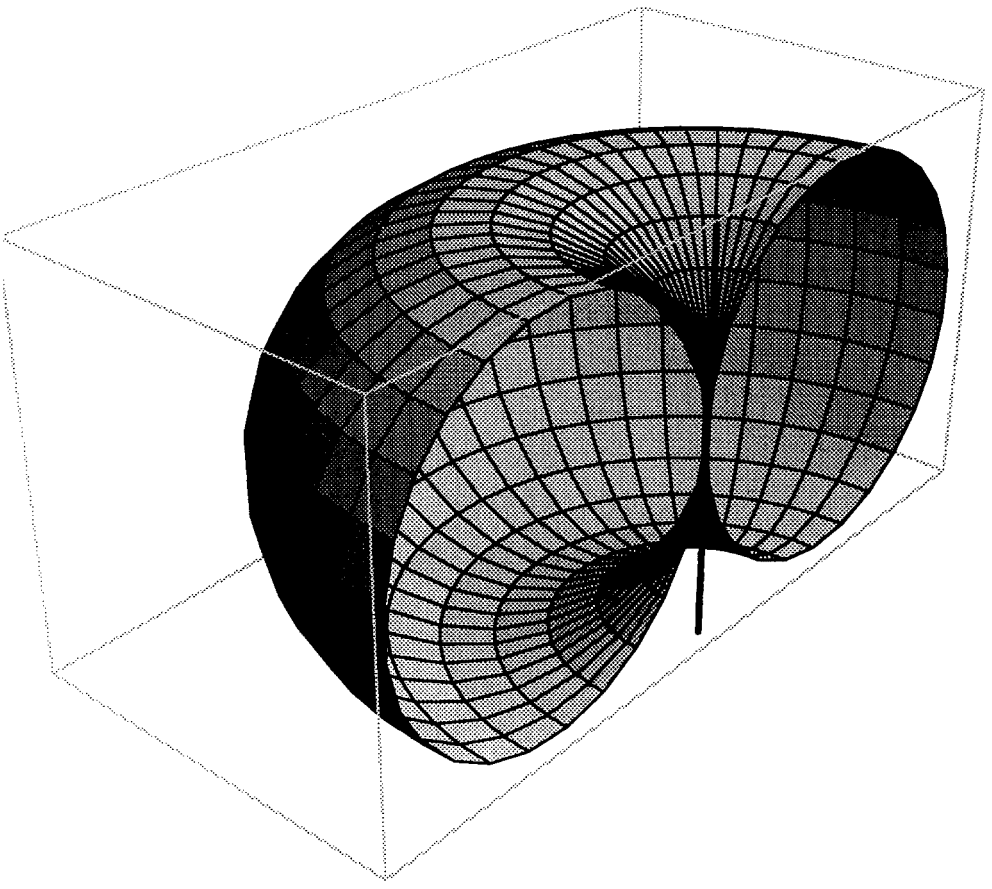

Fig. 1. Schematic diagram of the poloidal and toroidal modes which define a parametric surface (illustrated in the volume ($x \leq 0$) and shaded to give some indication of depth). The poloidal lines are vertical loops which have a common point at $(x, y, z) = (0, 0, 0)$, and the toroidal lines are horizontal, concentric rings. The individual modes are suitable for describing either electric or magnetic fields under restricted conditions. More generally, linear combinations of both modes are required to describe the EM fields in a complicated media or from an arbitrary source.

The source matrices clearly show which modes contribute to the behavior of particular field components (i.e., the T_n and P_n terms) and hence provide some intuition regarding the sensitivity of an experiment to layered earth structures. While the source matrices describe most of the difference between EM experiments, the characteristics of the modes themselves is also important. Consider, for example, the TM mode potential (T_n) which is proportional to $\alpha_{v,R}$, the admittivity of the media containing the receiver. When the physical realm is quasi-static $\alpha_{v,R} = 0$ if the receiver is located in the air layer. This implies that a source which generates a poloidal current can be located anywhere in or above the layered earth and not be detected by magnetic field measurements made external to the

conductive portion of the earth. Such a result may appear counter-intuitive until the reciprocal case is considered. A magnetic source (of any orientation) outside the layered earth can only generate horizontal current flow in the earth because of the boundary condition on vertical currents at the surface of the earth. Thus, there can be no poloidal current generated from this source. A cursory examination of the deep CSEM sounding literature and Table I shows that most experiments are based on 1D interpretations and ascribe all the observed EM response to either the PM or TM mode, but not both.

It is a simple matter to apply the principle of reciprocity to elements in Table I to deduce the relationships between sources and receivers. One example would involve relating the B_z field component from a horizontal electric dipole (HED) source in the x-direction (i.e. $I'_{x,e}$), to the E_x component of a vertical magnetic dipole (VMD) source ($I'_{z,m}$). From the tables one can derive that

$$\frac{E_x(I'_{z,m})}{i\omega\,\mathrm{d}A} = \frac{B_z(I'_{x,e})}{\mathrm{d}l} \qquad \text{so} \qquad E_x(I'_{z,m}) = B_z(I'_{x,e}) i\omega \frac{\mathrm{d}A}{\mathrm{d}l}.$$

Such relationships can be derived for any source/receiver pair and are quite helpful in discovering or rationalizing the behavior of a particular sounding experiment.

Another intended characteristic of the generalized representation is that the information about the continuation of the EM fields vertically between the source and receiver is contained in T and P. It is therefore possible to compare different source/receiver pairs which are not necessarily coplanar or in the same media. This isolation of the EM response function from source/receiver comparisons is a necessary consequence of the reciprocal nature of EM sources and fields.

Although this generalized representation is a useful basis for understanding EM sources and fields, it is mostly limited to qualitative comparisons. As an auxiliary aid for comparing different deep EM sounding methods, Table II contains a compilation of the EM fields from a VMD source and a HED source situated on the interface between the air and a uniform halfspace. The receiver is also situated on the interface. These expressions can be inverted to derive apparent conductivity functions and also demonstrate the general characteristics of the EM fields from a particular source. Table II can be augmented by Table I and reciprocity arguments to derive the fields from any other orientation of a dipole source. Furthermore, the general expressions in Table II can usually be transformed directly to the time domain and the appropriate limits taken for static (near-field) and (quasi-static) far-field conditions.

3. Sensitivity Analysis

An important, and sometimes neglected, aspect of controlled source EM work is sensitivity analysis. Sensitivity is defined as the amount of variation in the data

TABLE II

A compilation of the fields for EM dipoles situated on the interface between the air and a uniform halfspace. The fields are shown for three cases; the resistive or pseudo-static limit ($|\gamma_1 r| \ll 1$), the intermediate zone, and the far-field zone ($|\gamma_1 r| \gg 1$). The argument of the modified Bessel functions I_n and K_n is always $\gamma_1 r/2$ where $\gamma_1 = \sqrt{i\omega\mu_1\sigma_1}$

	VMD	HED
$E_r(\lvert\gamma_1 r\rvert \ll 1)$	0	$\frac{I\,dl}{\pi\sigma_1 r^3}\cos\phi$
$E_\phi(\lvert\gamma_1 r\rvert \ll 1)$	$-i\omega\mu\frac{I\,dA}{4\pi r^2}$	$\frac{I\,dl}{2\pi\sigma_1 r^3}\sin\phi$
$E_z(\lvert\gamma_1 r\rvert \ll 1)$	0	$i\omega\mu\frac{I\,dl}{4\pi r}\cos\phi$
E_r	0	$\frac{I\,dl}{2\pi\sigma_1 r^3}[1+(1+\gamma_1 r)\,e^{-\gamma_1 r}]\cos\phi$
E_ϕ	$-i\omega\mu\frac{I\,dA}{2\pi\gamma_1 r^4}[3-(3+3\gamma_1 r+\gamma_1^2 r^2)\,e^{-\gamma_1 r}]$	$\frac{I\,dl}{2\pi\sigma_1 r^3}[2-(1+\gamma_1 r)\,e^{-\gamma_1 r}]\sin\phi$
E_z	0	$i\omega\mu\frac{I\,dl}{2\pi r}I_1K_1\cos\phi$
$E_r(\lvert\gamma_1 r\rvert \gg 1)$	0	$\frac{I\,dl}{2\pi\sigma_1 r^3}\cos\phi$
$E_\phi(\lvert\gamma_1 r\rvert \gg 1)$	$-3\frac{I\,dA}{2\pi\sigma_1 r^4}$	$\frac{I\,dl}{\pi\sigma_1 r^3}\sin\phi$
$E_z(\lvert\gamma_1 r\rvert \gg 1)$	0	$i\omega\mu\frac{I\,dl}{2\pi\gamma_1 r^2}\cos\phi$
$H_r(\lvert\gamma_1 r\rvert \ll 1)$	$-\frac{I\,dA}{16\pi r^3}\gamma_1^2 r^2$	$\frac{I\,dl}{4\pi r^2}\sin\phi$
$H_\phi(\lvert\gamma_1 r\rvert \ll 1)$	0	$-\frac{I\,dl}{4\pi r^2}\cos\phi$
$H_z(\lvert\gamma_1 r\rvert \ll 1)$	$-\frac{I\,dA}{4\pi r^3}$	$\frac{I\,dl}{4\pi r^2}\sin\phi$
H_r	$-\frac{I\,dA}{4\pi r^3}\gamma_1^2 r^2[I_1K_1-I_2K_2]$	$\frac{I\,dl}{2\pi r^2}\left[3I_1K_1-\frac{r_1 r}{2}(I_0K_1-I_1K_0)\right]\sin\phi$
H_ϕ	0	$-\frac{I\,dl}{2\pi r^2}I_1K_1\cos\phi$
H_z	$-\frac{I\,dA}{2\pi\gamma_1^2 r^5}[9-(9+9\gamma_1 r+4\gamma_1^2 r^2+\gamma_1^3 r^3)\,e^{-\gamma_1 r}]$	$\frac{I\,dl}{2\pi\gamma_1^2 r^4}[3-(3+3\gamma_1 r+\gamma_1^2 r^2)\,e^{-\gamma_1 r}]\sin\phi$
$H_r(\lvert\gamma_1 r\rvert \gg 1)$	$-3\frac{I\,dA}{2\pi\gamma_1 r^4}$	$\frac{I\,dl}{\pi\gamma_1 r^3}\sin\phi$
$H_\phi(\lvert\gamma_1 r\rvert \gg 1)$	0	$-\frac{I\,dl}{2\pi\gamma r^3}\cos\phi$
$H_z(\lvert\gamma_1 r\rvert \gg 1)$	$-9\frac{I\,dA}{2\pi\gamma_1^2 r^5}$	$3\frac{I\,dl}{2\pi\gamma_1^2 r^4}\sin\phi$

produced by a perturbation in the model parameters. The mathematical device used to investigate sensitivity is the first order derivative of the model response (data) with respect to a model parameter (e.g. conductivity). This function is called a Fréchet derivative only if the higher order terms in the Taylor expansion can be shown to be second order, otherwise it is known as a Gateaux derivative. The distinction between Gateaux and Fréchet derivatives is important. Gateaux derivatives need not be linear or continuous meaning that higher order terms in the Taylor expansion can be significant and a linear approximation to the Taylor series may be invalid. 1D earth models have been shown to be Fréchet differentiable for various EM sources (e.g. Parker, 1977; Chave, 1984) as have a large class of 3D models for DC resistivity methods (Boerner and West, 1989c).

Fréchet derivatives, which play an important role in numerical inversion methods, are also useful for resolution studies (e.g. Gómez-Treviño and Edwards, 1983; Chave, 1984; Boerner and West, 1989b) and depth of investigation calculations (Spies, 1989). Fréchet derivatives have an interesting and useful physical interpretation. The original work on this physical interpretation by Gómez-Treviño (1987a) showed that the derivatives act as spatial weighting functions for conductivity and not just for perturbations in conductivity. That is, an integral equation relates the spatial distribution of conductivity to the EM data through the Fréchet derivative. For example,

$$\frac{\partial B_z}{\partial \ln \omega} = \int_v G_{B_z}(\mathbf{r}, \mathbf{r}', \sigma, \omega)\sigma(\mathbf{r}')\, \mathrm{d}^3 r', \tag{6}$$

where G_{B_z} is the Fréchet derivative of the vertical magnetic induction B_z with respect to $\sigma(\mathbf{r}')$. This mapping of conductivity to data means that data presentation schemes (e.g. apparent conductivity) can be understood by examining the spatial form of the Fréchet derivative. Of course, the Fréchet derivative is dependent on the conductivity model and hence the intrinsic non-linearity of the interaction between diffusive EM fields and conductivity structures is maintained. As well, it is important to remember that sensitivity analysis is only as accurate as the forward model, and is limited by the same computational restrictions. Fréchet derivative for 3D models are much more complicated than indicated by the simple one-dimensional analysis (Boerner and West, 1989c).

Figure 2 shows a perspective plot of the Fréchet derivative for apparent conductivity (derived from the magnitude of the ratio of H/E) given the step response excitation by a plane wave of a uniform halfspace. In essence, the Fréchet derivative shows that measurements at later time sample a broader region of the earth, but are centered at greater depths. Perhaps more importantly, the late time measurements are less biased by near surface structure than are early times measurements. Figure 3 shows the same type of plot for an impulsive plane wave source. For an impulsive source the apparent conductivity definition weights some

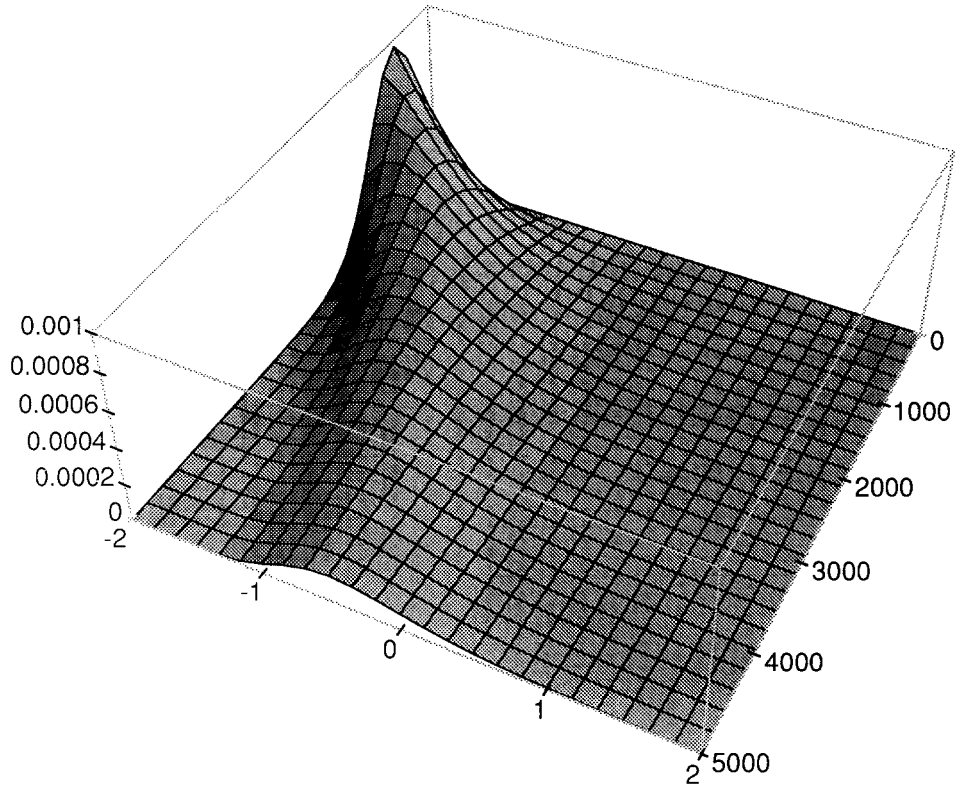

Fig. 2. The Fréchet derivative for apparent conductivity defined using H/E from a plane wave source over a uniform halfspace. The source is a step function in time and the surface elevation indicates the amplitude of the Fréchet derivative. The image shows the spatial weighting applied to the halfspace conductivity structure by the Fréchet derivative at different $\log_{10}$(times).

depths negatively, while the step response definition weights all depths positively. Frequency domain Fréchet derivatives are similar to those of the impulse response in that some depths are weighted negatively, but they do not show decreased sensitivity to surficial features at longer periods. Gómez-Treviño (1987b) used the example of negative spatial weighting to conductivity to illustrate how the apparent conductivity definitions can lead to the overshoot/undershoot problem often encountered in EM methods.

Figures 2 and 3 indicate how different measurements with the same source and receiver can result in disparate apparent conductivity definitions (see also, Spies and Eggers, 1986). It is not possible from these plots to determine the Fréchet derivatives of more complicated media. The PM (inductive) mode Fréchet derivatives for controlled and natural source EM methods are only weakly dependent on the earth model (Boerner and Holladay, 1990). Gómez-Treviño (1987a) was able to approximate the halfspace magnetotelluric (MT) Fréchet derivative with a boxcar function and derive the Niblett–Bostick transform (Jones, 1983a). The

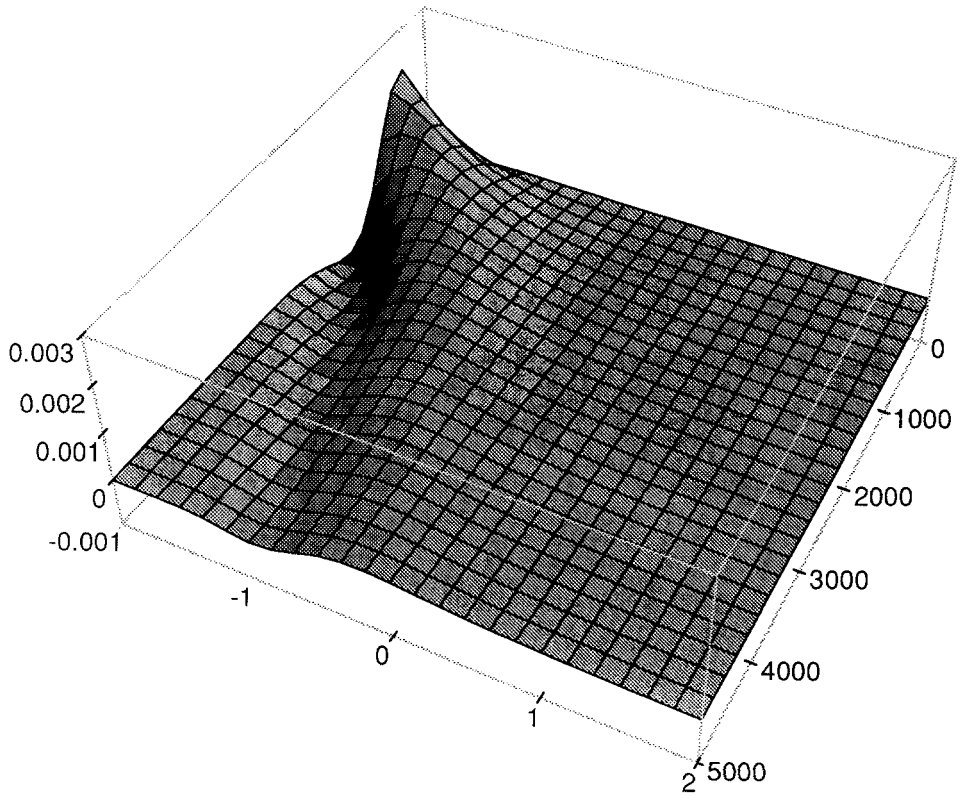

Fig. 3. The Fréchet derivative for apparent conductivity defined using H/E from a plane-wave source over a uniform halfspace. The source response is an impulse function and the surface elevation indicates the amplitude of the Fréchet derivative. The image shows the spatial weighting applied to the halfspace conductivity structure by the Fréchet derivative can obtain negative values (unlike the step response source function).

implication for PM mode CSEM measurements is that the Fréchet derivative of some representative earth model (e.g. a uniform halfspace) could be used in designing simple transformations or data "imaging" schemes (e.g. Nekut, 1987; Macnae and Lamontagne, 1987; Eaton and Hohmann, 1989). In contrast, TM mode Fréchet derivatives are usually quite model dependent (Boerner and West, 1989b) and are probably less amenable to simple conductivity mapping methods.

This simplistic overview of Fréchet derivatives raises some important questions about the "proper" definition of apparent conductivity and the subsequent interpretation of structure, particularly when comparing results from different experiments. Although data comparisons through apparent conductivity may be useful in some cases (e.g. Sternberg *et al.*, 1988), a preferable alternative to apparent conductivity definitions would be to compare models derived from inversion. When the model space is properly explored as part of the inversion, the inherent differences between various data should have minimal affect on the interpreted

structure (but may strongly affect the resolution). As inversion is not currently practical for 3D data, image techniques and/or apparent conductivity will continue to be an important part of interpretation. These results should be viewed with caution however, and interpretations based on such information should be confirmed (as far as possible) by forward modelling.

4. Three Dimensional Conductivity Structures

The generalized representation of EM source fields is an attempt to alleviate some of the conceptual difficulty in understanding 3D sources. However, it is much more difficult to generalize the interaction of finite sources with 3D conductivity distributions. Without attempting to develop the theory for 3D modelling, the discussion in this section will be limited to qualitative descriptions of the influence on CSEM responses by three dimensional structure.

Multi-dimensional modelling for controlled source methods is in a very elementary state. Algorithms for 2D and 3D model responses are necessarily difficult to develop, program and compute because it is not generally possible to model all aspects of 3D CSEM sources with 1D or 2D representations (e.g. Nabighian and Oristaglio, 1984), although there are certain special cases (e.g. Goldstein and Strangway, 1975; Lienert and Bennett, 1977).

Despite these difficulties with 2D and 3D models, a number of useful techniques have been produced for computing the EM response of various multidimensional models (see Varentsov, 1983). These methods include finite element (e.g. Pridmore *et al.*, 1981; Gupta *et al.*, 1989), finite difference (e.g. Oristaglio and Hohmann, 1984), integral equation (e.g. Raiche, 1974; Hohmann, 1975; Weidelt, 1975; Newmann *et al.*, 1986), hybrid methods (e.g. Lee *et al.*, 1981; Gupta *et al.*, 1987) and thin sheets (e.g. Vasseur and Weidelt 1977; Vanyan *et al.*, 1987; Smith and West, 1987). Of the available methods, the integral equation approach is often preferred because only the anomalous conductivity volume, V, need be discretized. Integral equations also provide some insight into the 3D scattering of EM fields and hence will be the focus of this discussion.

In a simple generic form, the physics of the interaction between a wave field obeying the Helmholtz equation and some scattering object can be expressed as a Fredholm integral equation of the second kind which must be solved in V or on the surface bounding V,

$$F(\mathbf{r}) = F(\mathbf{r})^{\text{Host}} + \int_V G(\mathbf{r}|\mathbf{r}')F(\mathbf{r}')P(\mathbf{r}')\,d\mathbf{r}'. \tag{7}$$

Here $F(\mathbf{r})^{\text{Host}}$ is the field measured at the observation point $\mathbf{r}$ which would exist in the absence of any scattering structure. $F(\mathbf{r}')$ is the field which is scattered from the inhomogeneity and $G(\mathbf{r}|\mathbf{r}')$ is the host medium Green's function. The physical

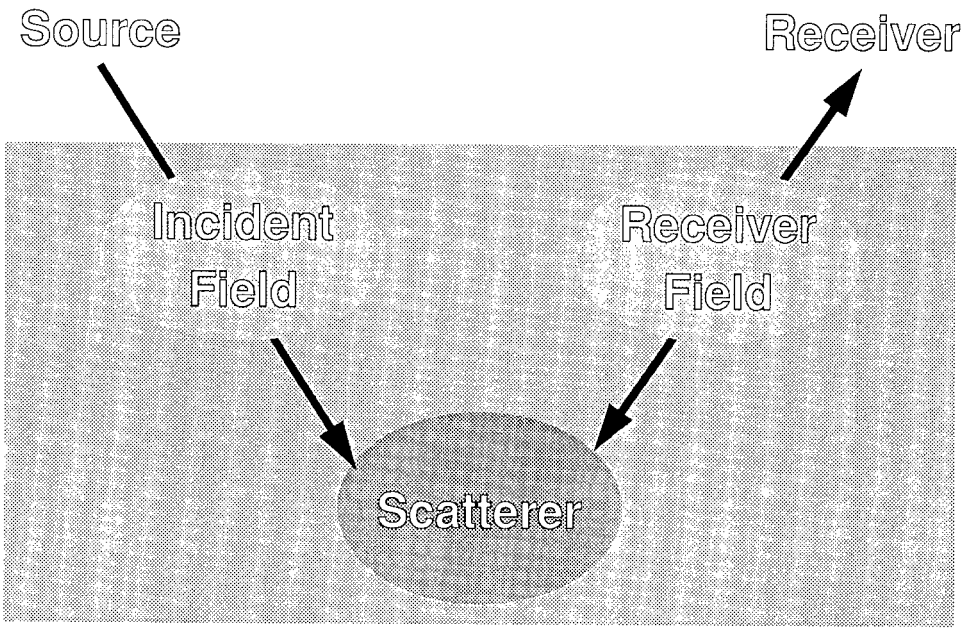

Fig. 4. Schematic diagram representing the essential components of the integral equation method for a scattering feature embedded in the earth (gray region). In this diagram, the source and receiver are assumed to be external to the earth. The "incident" and "receiver" fields are simply the host Green's functions representing the continuation of the EM fields between different depths and are independent of the scattering feature. Similarly, once the host is specified, it is possible to derive a transfer relationship between a set of unspecified incident field and the equivalent currents. Thus, the integral equation model can logically be divided into two parts which can be computed separately and recombined for different source/receiver types and geometries (but for a single body model and host structure).

properties of the scattering feature, relative to the properties of the host, are represented by $P(\mathbf{r}')$. A physical interpretation of (7) is that $F(\mathbf{r}')P(\mathbf{r}')$ represents a set of "equivalent" sources which, when placed in the host medium, reproduce the EM response of the scattering body. In fact, the integral equation method is sometimes referred to as the "equivalent source" technique.

Integral equations are based on the duality between boundary conditions and sources; boundary conditions can be replaced by sources, and vice versa. In this regard, integral equations represent a slightly different physical emphasis on EM scattering from the Helmholtz equation. A simple dimensional analysis of the incident and scattered field from an integral equation for electric field indicates why current channelling numbers (e.g. Edwards, 1975; Jones, 1983b) are important for describing the behavior of electric current near anomalous conductivity structures. On the other hand, a dimensional analysis of the homogeneous Helmholtz equation suggests the importance of induction number parameterization.

The basic physics described by integral equation methods can be represented schematically by Figure 4. Three components are displayed in this diagram: the

electric field created on the scattering structure by the source field, the scattering currents in the body and/or host which are required to maintain the boundary conditions, and the fields from the source and scattered currents which are observed at the receiver point. Host models are usually one-dimensional because the EM Green's functions for such structures can be found analytically. The arrows in this figure point between the source and receiver. A useful variation on this diagram is to replace the receiver by its reciprocal source and find the electric field incident on the scattering body (indicated by the double headed arrow). Reciprocal sources are often used in numerical modelling to reduce the computational burden of computing the Green's functions. Notice that both the source and receiver must have favourable "coupling" with the feature in order to have a detectable EM response which indicates an intimate tie between integral equations and sensitivity analysis (Boerner and West, 1989c). That the source coupling to known structure (e.g. near surface features) can be maximized or minimized represents an important advantage of CSEM methods over natural source techniques.

The simplified conceptual model of the IE method shown in Figure 4 can be quite useful. An important and relevant example was given by West and Edwards (1985) who show that if the scattering body is small compared with the wavelength of the source field, it may be sufficient to represent the scattered (equivalent) currents with purely galvanic current flow. That is, the frequency response of the 3D earth is determined entirely by the frequency response of the 1D host because the response of the body is essentially galvanic. If the scattering body is near surface, there may be little attenuation of the incident and scattered Green's functions in the frequency bandwidth of interest and the response of the body would appear static.

Figure 4 also emphasizes that all EM experiments theoretically have the same receiver sensitivity to 3D structure. The difference lies in how the incident field is impressed on the scattering feature by the source field. As an example, consider the electric fields induced in a layered earth by a linearly polarized plane wave source and by a horizontal electric dipole (schematically illustrated in Figure 5). The plane wave source induces an electric field linearly polarized in one direction, in contrast to the electric field created by the dipole source which is a strong function of radius and frequency. In general, it is only along certain lines of symmetry that **E** from a HED is linearly polarized. The far-field response of the dipole source is linearly polarized but the orientation of the major axis is dependent on the angle between the source and receiver. Thus, the electric field from the dipole which is incident on the scattering body is usually different geometrically, and sometimes different temporally, from plane wave induced fields.

Ward (1983) illustrate these affects by computing numerically the response of a grounded bipole or loop located near a sedimentary basin. When the grounded bipole source is oriented across the basin, the conductive sediments represent a

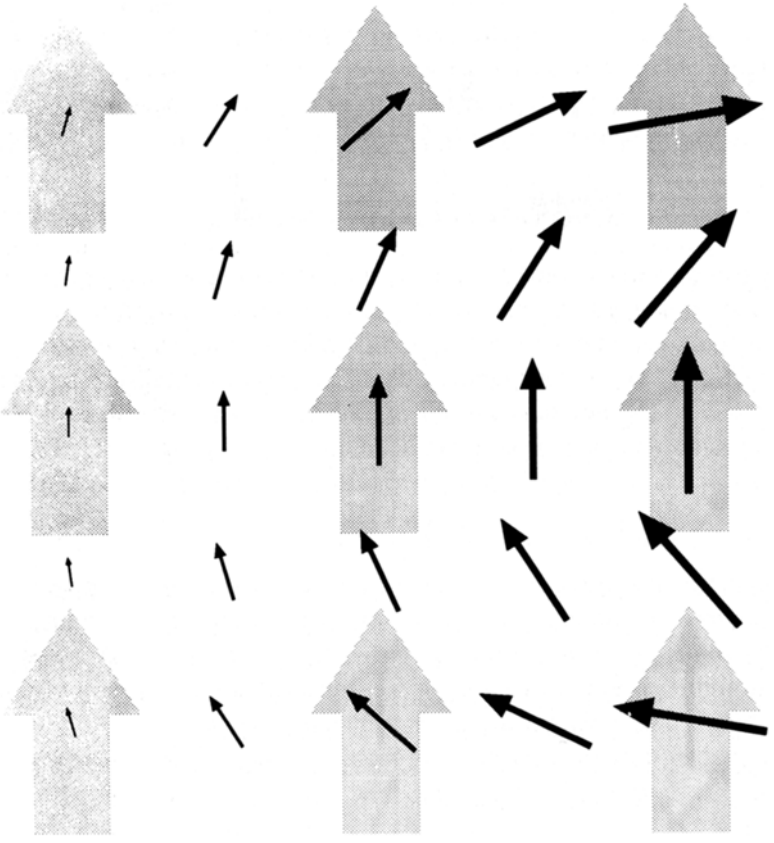

Fig. 5. Schematic diagram of the electric field created by a linearly polarized plane wave source (large gray arrows) and the electric field of a HED (small black arrows). This illustration is a qualitative representation of the incident electric field "couples" differently in a geometrical sense with scattering body depending on the type of source.

"short circuit" between the grounding points of the bipole and distort the source field. A different distortion was produced by having the source parallel to the structure, but not crossing it. These effects have serious implications for interpretation and must be accounted for with modelling when recognized. Clearly the transmitter site for any CSEM experiment should be carefully chosen to minimize such responses.

Complicated 3D modelling may not always be necessary if the scattering is from a structure local to the transmitter or receiver and is essentially galvanic. In this case, the effect at DC could be modelled as simply a "static" change in the source current, or receiver moment. A useful and often applied method in CSEM to account for such shifts uses the DC response of H_z from a grounded bipole which is independent of layered earth structure. Accurate 1D interpretations can often

be obtained if the level of the data curves is normalized to this DC limit to account for amplitude offsets due to surficial features (Newman, 1989). Such normalization has the additional benefit of accounting for receiver mis-location and inaccuracies in estimates of the source current (e.g. Gómez-Treviño and Edwards, 1983).

5. Results of Deep Controlled Source Soundings

It is impossible to devote adequate space in this review to a thorough analysis of all the deep controlled source sounding experiments reported in the literature. Instead, a few experiments which are illustrative of particular concepts in deep sounding CSEM will be highlighted in the following sections. In particular, the discussion will be categorized in terms of advantages and difficulties of controlled source methods. The themes of these sections are admittedly generalizations but should provide some insight into the utility and analysis of CSEM methods.

5.1. Spatially localized source fields

In the general quasi-static realm, the EM fields of dipole sources are a strong function of lateral wavenumber. This wavenumber response is manifest in the space domain (Table II) as an inverse power law fall-off of amplitude with radial distance from the source. Since an EM receiver is also a reciprocal source, all EM fields scattered from a 3D feature are subject to this geometric fall off. Controlled source methods differ from natural source techniques in that the excitation field also has a strong lateral decay and which effects the data even for layered earth models.

Geometrical decay of the source fields may be beneficial when large scale (regional) structures are adjacent to the sounding location. When the coupling of the source with regional structures can be minimized, this capability of CSEM methods can partially offset the lack of sophisticated modelling tools. There is, however, an important trade-off to consider because of the radial decay of the artificial fields. Since natural source fields are thought to be relatively uniform over a large area and predominantly horizontal, the signal to noise ratio for a controlled source sounding is poor in the horizontal components and usually decreases with increasing offset from the source. Furthermore, the natural signal is non-stationary and hence stacking of the controlled source data does not necessarily give $\sqrt{N}$ improvement. It is for this reason that Wilt *et al.* (1983) and Spies (1988) advocate techniques which use a magnetic field reference to cancel the low frequency natural field variations in the controlled source measurement. At the long periods used for deep sounding, this is particularly important because the natural spectrum increases in amplitude as approximately $1/f^2$. Such noise cancellation methods have the additional benefit of producing a resultant noise spectrum which appears to be almost white (Nicholls *et al.*, 1988).

One experiment where the limited extent of the source fields was used to

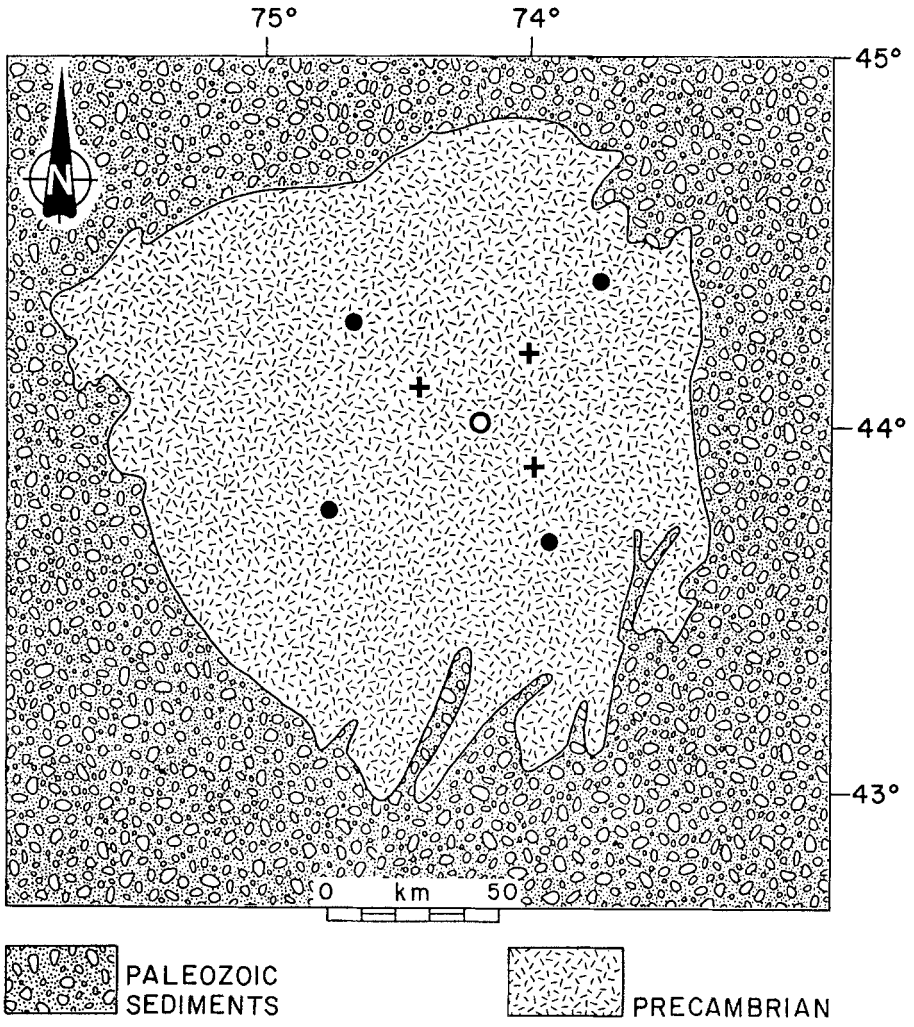

Fig. 6. A generalized geology map of the Adirondack dome indicating the location of the source and receiver sites. The Precambrian uplift is surrounded by an accumulation of Paleozoic sediments which thicken to the south. The source location is indicated by the circle, the plus signs indicate CSEM receiver sites and the solid dots represent CSEM receiver sites and horizontal spatial gradient measurement stations.

advantage was reported by Connerney *et al.* (1980). A loop source (VMD) having a moment of (65A) $\times$ (14.6 $\times$ 10^6 m^2) $\approx$ 10^9 A m^2 was used to probe the Precambrian shield in the northern New York State Adirondacks. This uplift is dome-like, nearly circular, approximately 200 km in diameter and is surrounded by surficial deposits of conductive Paleozoic sediments. Sediment accumulations are thickest to the south of the dome. The transmitter location for deep sounding was chosen near the geometrical center of the dome (Figure 6).

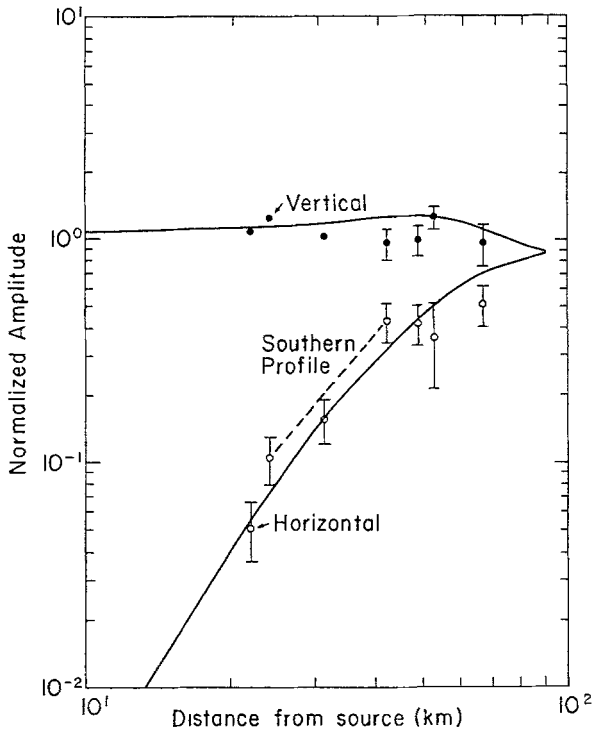

Fig. 7. Vertical and total horizontal magnetic fields reported by Connerney *et al.* (1980) over the Adirondack dome at 0.05 Hz. The accepted model response is plotted with solid lines. The dotted lines indicate stations situated in the south-east portion of the dome near the thickest accumulation of Paleozoic sediments.

Three components of the magnetic field were recorded at periods ranging from one to twenty seconds transmitted from a source loop, approximately 4 km in diameter. Receiver separations from the center of the source loop ranged between 20 and 65 km. Figure 7 shows the amplitude of the vertical and total horizontal magnetic fields observed for a source waveform period of 20 seconds. The data are normalized by the fields of a magnetic dipole in free space and the data are shown as symbols (solid dots for H_z and open dots H_r) with the EM response of the accepted model plotted as solid lines. As the distance from the source is increased, the magnetic field tilts from the vertical towards the horizontal. The 1D model response indicates that separations of well over 100 km would be required to be in the plane wave field of this source (i.e. when $H_r \gg H_z$) at 20 s periodicity.

Near the source, the horizontal field component is much smaller than the vertical component and is contaminated by larger components of natural signal. However, the horizontal field is generated purely by induction and consequently is more sensitive to changes in conductivity with depth than the vertical field (which has a primary component from the source). The combination of sensitivity and low

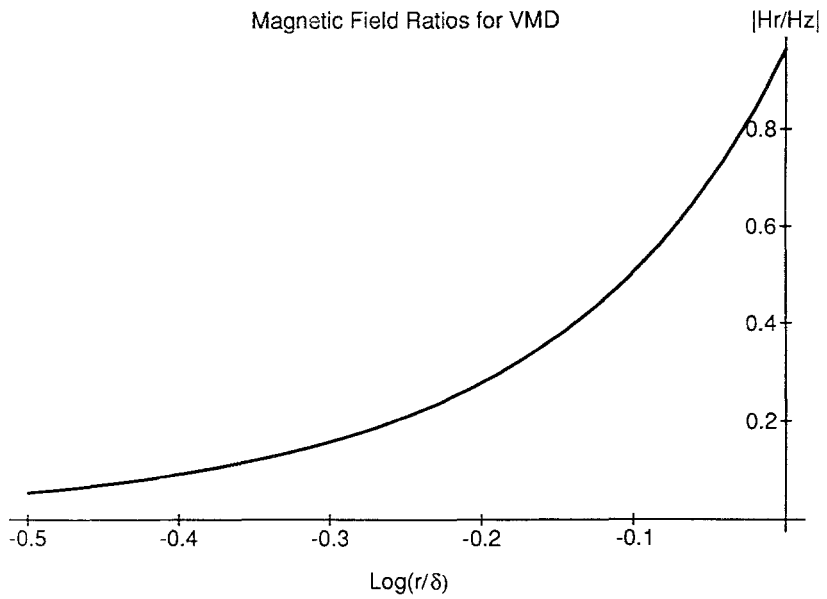

Fig. 8. The magnitude of H_r/H_z computed for a uniform halfspace as a function of $\log_{10}(r/\delta)$, where δ is skin depth. This curve can be used to estimate the apparent conductivity from the magnetic field ratios for a magnetic dipole source.

amplitude is a concern because non-orthogonality or inclination of the EM source and/or receiver will introduce signal into the radial magnetic field measurement (see Wilt *et al.*, 1983 and Fullagar and Oldenburg, 1984). If this extra signal is not accounted for in modelling, it will erroneously be interpreted as a conducting layer. In this fashion, magnetic field measurements from an inductive source can be strongly susceptible to mis-orientation due to local topography.

Figure 8 illustrates the magnitude of H_r/H_z for a uniform halfspace as function of source/receiver separation normalized by skin depth, that is, r/δ where $\delta = \sqrt{2/\omega\mu\sigma}$. To satisfy the data of Connerney *et al.*, the ratio H_r/H_z must be approximately 0.5 at 0.05 Hz with the receiver 50 km from the source. These values implies that r/δ is approximately $10^{-0.1}$ which in turn yields an apparent conductivity of almost 10^{-3} S/m, at least an order of magnitude larger than the 10^{-4} S/m found from higher frequency (shallower) EM data by Nekut *et al.* (1977) and DC resistivity soundings performed by Cantwell *et al.* (1964) and Anderson and Keller (1966). While this simplistic calculation does not provide an interpretable result, it is clear the low frequency EM data support the notion of an increase in conductivity at depth. However, an important question is whether the conductive sediments surrounding the dome are responsible for the observed response, or is it some deep layer? Given the location of the source and the lateral distance between the furthest station and the sediments, it seems unlikely that these sediments are capable of generating such a large horizontal magnetic field.

This bold, qualitative statement could be verified to some extent by examining the data for indications of 3D effects. At large offsets compared to the source loop size on a 1D earth, the horizontal magnetic field is purely radial from the source center. Some researchers (e.g. Wilt *et al.*, 1989) have used the magnitude of the ratio $|H_\theta/H_r|$ to indicate deviations from one dimensionality, but Connerney *et al.* (1980) do not present or discuss the H_θ data. For this particular experiment the gross structure of the surficial conductivity is approximately concentric about a VMD source and H_θ may not be a useful indicator of lateral structure.

Another dimensionality test is to compare the soundings from various radial profiles extending outward from the center of the dome. On a 1D earth (or cylindrically symmetric earth, concentric with the source) these profiles should all be identical. However, when the data is grouped geographically there is a trend of increasing conductivity (larger horizontal magnetic field at the same separation) towards the thicker sediments in the southern part of the dome (dotted lines in (7)).

In an attempt to resolve the influence of the lateral conductivity structure for this sounding, the horizontal magnetic field observed on a radial profile away from a magnetic dipole source situated on an inhomogeneous thin sheet (Vasseur and Weidelt, 1977) was computed (Figure 9). The center of the sheet has a conductance of 1 S, while the exterior of the sheet was either 1, 10 or 50 S. The data points in (Figure 9) are those reported by Connerney *et al.* (1980) and it is certain that, while the sediments may affect the data for stations near the edge of the dome, the magnitude of the horizontal magnetic field is not explained by the lateral structure alone. Thus, it appears that the limited spatial source field permitted sounding through a resistive "window" to detect a conductive layer in the lower crust.

The natural source soundings in this region principally consists of horizontal spatial gradient (HSG) work by Connerney and Kuckes (1980), as well as some longer period geomagnetic variation studies (Greenhouse and Bailey, 1981). The Connerney and Kuckes (1980) work is more relevant and indicates the top of a conducting layer at a slightly greater depth (30 km) than the controlled source work (23 km). HSG processing relies on the assumption that the only natural magnetic field in the vertical direction is caused by a gradient in the source field (e.g. Berdichevsky *et al.* (1969), Schmucker (1970); see also Fiskina *et al.* (1986) who discuss HSG for CSEM). The discrepancy between the HSG and CSEM may be the contribution due to lateral current flow induced in the Paleozoic sediments creating an anomalous H_z field. The four stations used in the HSG analysis were all less than 40 km from the edge of the sediments. Certainly both data sets are influenced by the sediments, although the HSG is probably more sensitive to this lateral structure. Without further modelling of the natural source experiment, it is difficult to be confident in the 1D HSG interpretation and correlation with the CSEM.

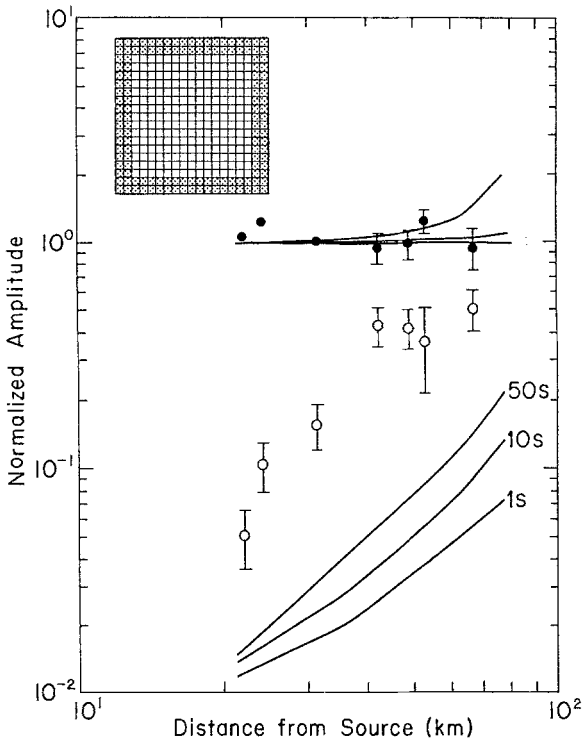

Fig. 9. A model study of an inhomogeneous thin sheet which is resistive in the center, but has higher conductance on the exterior. The conductance of the exterior part of the sheet was 1, 10 or 50 S. The data of Connerney *et al.* (1980) at 0.05 Hz are also plotted.

5.2. Source moment

The strong geometrical decay of controlled source fields has quite naturally resulted in efforts to increase the source moment (e.g. Keller *et al.*, 1984, Velikhov *et al.*, 1986). Equation (5) shows that increasing the source moment proportionally increases the amplitude of the EM fields. There are two methods of increasing the source moment; increasing the source current, and increasing the length (or area) of the source. The current strength can be easily increased to rather large values but is then constrained by the cost and weight of the transmitter system, by the difficulties of controlling the high power switching electronics required for a periodic source, and by safety considerations. While extracting low level signals from a high-noise environment is an attractive compliment to increasing the source moment (Section 5.1), it is not an alternative. In general, the time-averaged moment of the EM source must be large enough to permit adequate penetration of the fields and recovery of low amplitude signals through data processing.

5.2.1. *Source Current Strength*

Astrakhantsev *et al.* (1979) used a magnetohydrodynamic (MHD) generator to generate current for a one kilometer square wire loop near Sverdlovsk in the

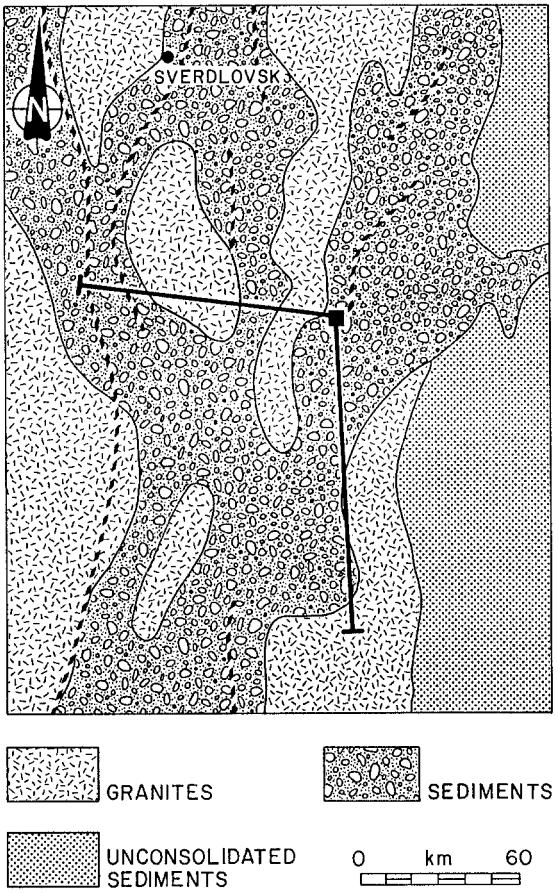

Fig. 10. A simplified geology map in the region of the MHD study by Astrakhantsev *et al.* (1979) illustrating the complicated geoelectric structure in the vicinity of the EM sounding. The square indicates the source location while the solid lines indicate the two profiles discussed in the text.

eastern Urals (Figure 10). The MHD generator essentially transforms plasma energy into a Hall current which can be fed into a loop or grounded source wire. The advantage of MHD sources is the tremendous output power which can be generated relative to the physical size and weight of the generator. However, the current waveform is not easily controlled and deconvolution of the source response is essential. For this survey, data were collected with a narrow band receiver at individual frequencies and source deconvolution reduced to normalization by the current amplitude.

The MHD generator achieved a source moment of $(3.8 \times 10^4\ \text{A}) \times (10^6\ \text{m}^2) = 3.8 \times 10^{10}\ \text{A-m}^2$ and the field components observed were E_ϕ, E_r, H_r and H_z up to 88 km from the loop source. While this source moment is only 40 times greater than Connerney *et al.* (1980) obtained, the source area was 15 times smaller. Since

the source was "fired" only occasionally, the time-averaged moment of the source may be comparable to that of Connerney *et al.*

Figure 11 shows the distribution and length (scaled by r^2) of the electric field measured around the loop source. There are clearly strong lateral affects in the electric fields, particularly in the amplitude, although the orientation of the vectors is also disturbed (Table II indicates that the electric field should be oriented in the θ direction). The surficial geology in the survey area consists mostly of sedimentary rocks with granitic basement exposed in several locations. Such structures can be expected to have relatively large lateral conductivity contrasts which probably generate the strong variations in the electric field amplitude and direction.

The erratic behavior of the electric field data caused Astrakhantsev *et al.* (1979) to interpret only the magnetic field data, however the lateral geological heterogeneity implied by the **E** data should be kept in mind during the interpretation. Under the assumption that $|\gamma_1 r| \ll 1$, and apparent conductivity for the MHD data was defined from the ratio $|H_r/H_z|$. For small induction numbers, H_r is proportional to $\omega\sigma/r$ on a halfspace, while H_z is proportional to just r^{-3}, even on a layered earth. This situation is known as sounding in the resistive limit (e.g. Esparza and Gómez-Treviño, 1987), and including H_z in the apparent conductivity definition is meant to account for uncertainties in site location and in the source current strength (but not for scattered fields).

Figure 12 is a plot of apparent conductivity for the two radial profiles (shown in Figure 10) reported by Astrakhantsev *et al.* (1979), each of which show markedly different features. The solid line in this figure is a synthetic sounding curve for a layered earth expressed (apparently) as a resistive limit apparent conductivity. The distortions in the NS profile are due to surficial inhomogeneities as confirmed by shallow soundings. H_z, which becomes independent of $\sigma(z)$ as $\omega \to 0$, is not significantly different from the theoretically predicted field, signifying only small scale 3D scattering. On the EW profile, H_z is severely disturbed and is a factor of 1.5 smaller than predicted. The anomalous H_z field correlates with a strong increase in the amplitude of the horizontal magnetic field giving a large apparent conductivity. This feature is interpreted as a fault by Astrakhantsev *et al.* (1979) and is thought to strike NS. The dip of the fault was estimated at 45° from the deep soundings and shallow inductive source soundings where the fault is exposed. Without data at several frequencies, or multiple source/receiver sites near the postulated fault zone, the conclusions regarding the nature of the fault are difficult to verify. Such a conductive and elongated feature should be an effective current channel and would be evident in the electric field data.

The assumption of small induction numbers used for deriving the apparent conductivity should be confirmed (or refuted) to determine the validity of the apparent conductivity definition. Figure 13 shows the correction factor that would have to be applied to the apparent conductivity definition used by Astrakhantsev *et al.* (1979) as a function of normalized distance. The small induction number

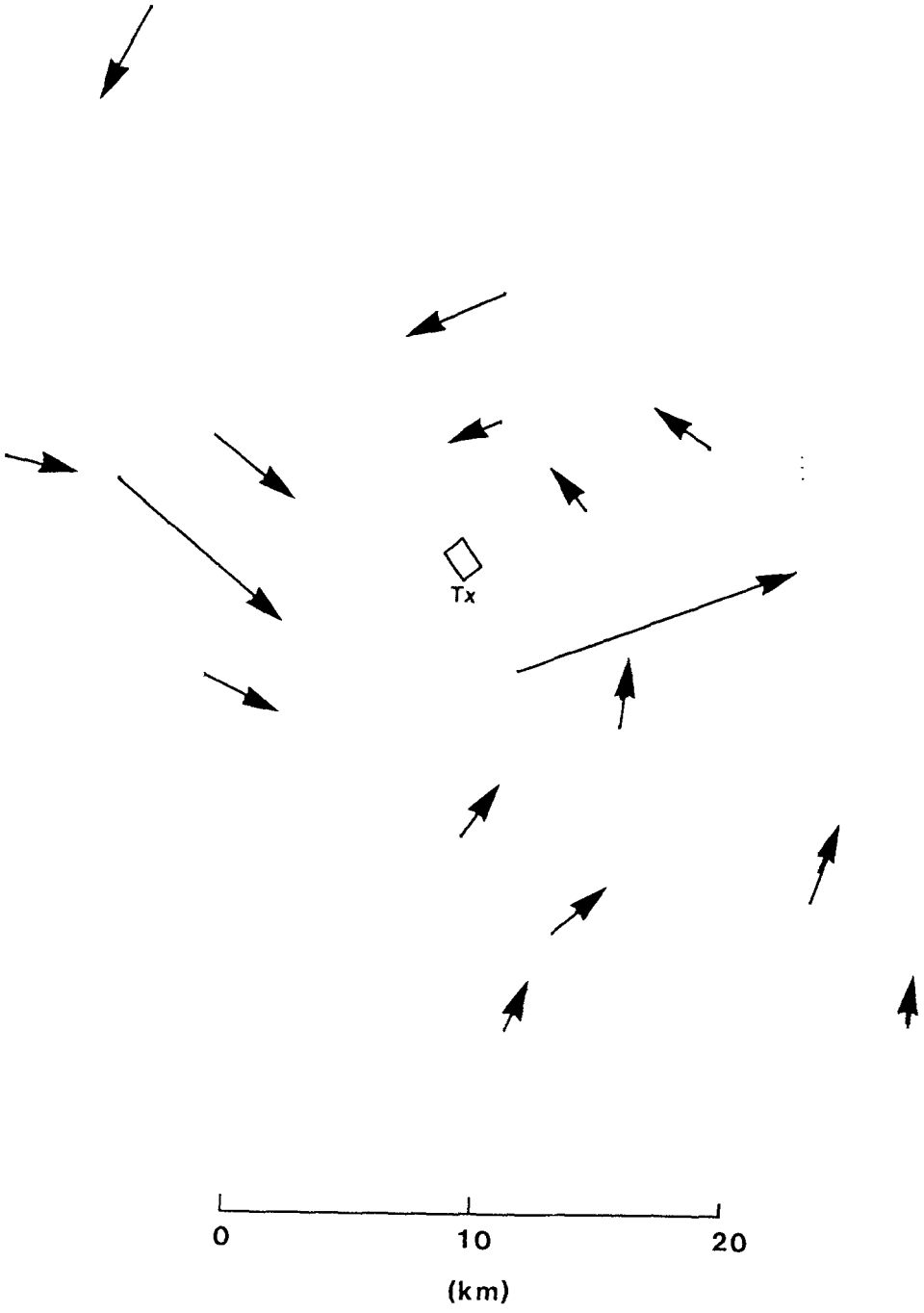

Fig. 11. The distribution of the near source measurement stations around the VMD source used by Astrakhantsev *et al.* (1979) showing the scaled electric field vectors (plotted as $|E|r^2$).

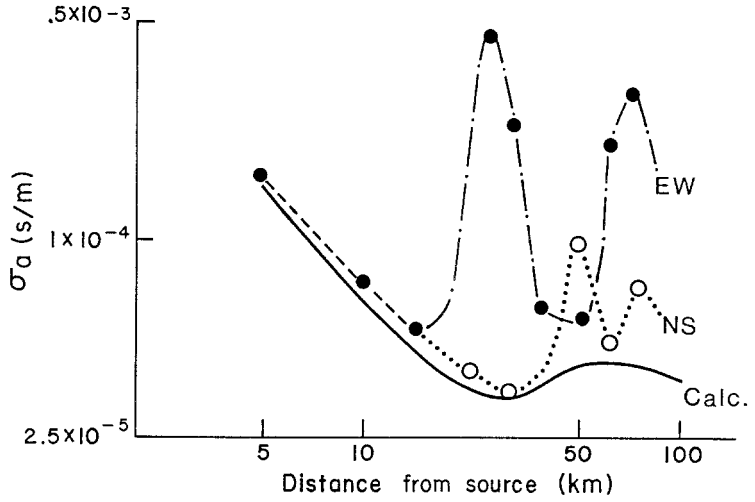

Fig. 12. Two apparent conductivity profiles from Astrakhantsev *et al.* (1979) defined for data acquired in the resistive limit. The solid line is the theoretical apparent conductivity for a preferred model while the dotted lines are from data measured on two profiles away from the source.

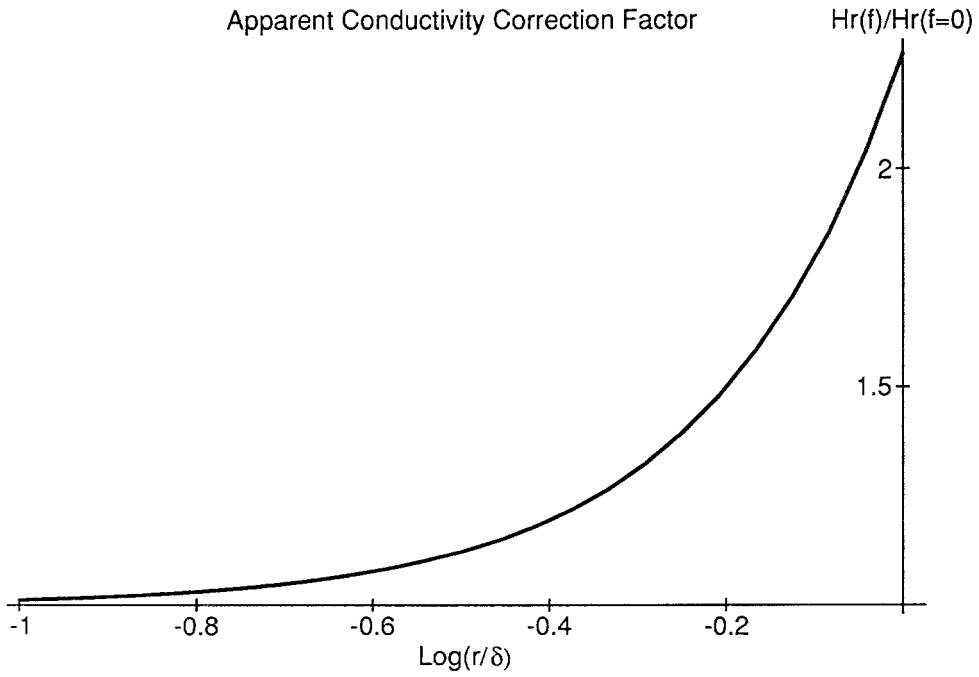

Fig. 13. Correction factor required to adjust the level of the resistive limit apparent conductivity calculations used by Astrakhantsev *et al.* (1979) when $|\gamma_1 r|$ is not necessarily small. The correction values are plotted as a function of $\log_{10}(r/\delta)$.

assumption is valid when the correction factor is approximately one. This plot indicates that saturation begins to limit the amount of current induced in the halfspace as $|\gamma_1 r| \to 1$. In contrast, the small induction number limit implies H_r is proportional to frequency, so apparent conductivity defined for data which exhibit the saturation response (i.e. $|\gamma_1 r|$ is of order 1) must be biased downwards. At 1 Hz, $r = 30$ km, and $\sigma = 5 \times 10^{-5}$ S/m, $r/\delta \approx 10^{-0.37}$ and hence the apparent conductivities reported by Astrakhantsev *et al.* (1979) may be too small at the most distant stations.

A conductivity-depth section was interpreted by examining the geometrical behavior of the magnetic fields along the NS profile and then using 1D forward and inverse modelling. The resistive middle crust is probably not well resolved by the magnetic field data alone (since it is purely PM mode), but an upper limit on the conductivity of resistive layers can usually be established with some certainty. The CSEM data support an increase in conductivity with depth, with a much more conductive lower crust than indicated by the apparent conductivity. However, the authors report that MT sounding results (unreferenced) indicate a longitudinal conductance of 50–150 S (to an unspecified depth in the crust) in this area, while the CSEM suggests only 0.7–3.5 S. This two order of magnitude difference is disconcerting. Without knowing if the MT curves were shifted to a deep conductivity reference curve or corrected in some other manner for static distortions, it is difficult to compare the the 1D interpretation of both methods. Static effects are relatively small in the controlled source data (i.e. at most a factor of 1.5 in H_z (on one profile) and the electric fields were not used in the interpretation) and so the conductance determined by CSEM may be more appropriate for the upper crust.

5.2.2. *Source Dimensions*

Logistics are often more important in determining the spatial extent of the source than experimental design. As well, there is a point of diminishing return when extending a source length to increase the moment because of the geometric fall-off from the far ends of the bipole. In general, the source achieves only an "effective" moment, determined by the 2D limit. An important consideration in increasing the source dimensions is that it becomes increasingly difficult to find geologically homogeneous regions in which to place the source.

One important method of obtaining extremely large source dimensions takes advantage of unused telephone or power lines (e.g. van Zijl, 1969; van Zijl *et al.*, 1970; van Zijl and Joubert, 1975; Blohm *et al.* 1977; Duncan *et al.*, 1980; Constable *et al.*, 1984). This can permit current electrode separations exceeding several hundreds of kilometers. The major difficulty with using available man-made structures for EM sources is that the transmitter invariably crosses different geological terrains and may not be suitably placed to reduce the EM response of regional structures or to test the dimensionality of the earth. van Zijl and Joubert (1975)

reported three soundings in South Africa which were centered on exposed granitic basement, but extended past the boundaries of these tectonic areas. To demonstrate lateral uniformity in the vicinity of the receiver, the typical in-line Schlumberger configuration was modified by locating the receiver some tens of kilometers on a perpendicular bisector from the transmitter. There was very little change in the apparent resistivity curves suggesting local homogeneity near the bipole center. Considering the reciprocal nature of EM sounding, it should be equally important to show that the location of the current electrodes did not produce the lower potential recorded at large offsets (this is usually done by conducting two soundings in nearly orthogonal directions). Of course, these experiments were performed where transmission lines are available and independent dimensionality checks may be impossible. It is perhaps significant that the sounding curves obtained by van Zijl and Joubert (1975) from quite different geological settings are all very similar (as are the results from other deep soundings in South Africa) and this provides confidence in their interpretations.

Lienert and Bennett (1977) and Lienert (1979) report on EM soundings made from a 2D source. In these experiments, the horizontal and vertical magnetic fields were observed from a 1400 km long power line near the northwest portion of the Basin and Range province (Figure 14). The source carried a square wave current of 270 to 298 A. Amplitude and phase of the signal at the fundamental plus the odd harmonics of the square wave at a period of 600 seconds were recorded up to 70 km from the power line. The data were interpreted in terms of image theory and layered earth models, but in both cases, the source was modelled as an infinite line current. Numerical models using Lienert and Bennett's interpreted conductivity structure for a 1D earth suggests that it is sufficient to model the source as 2D when the site is more than 400 km from a grounding point (this may invalidate some of Lienert's (1979) interpretations as his profiles extend to within 75 km of a grounding point). However, the affects of current channelling in the data should be addressed before interpretation with simplistic models.

The amplitude data from Lienert and Bennett's (1977) profile are remarkably symmetric about the source and do indicate a trend of increasing conductivity detected at longer periods (Figure 15). The phase data show more scatter and less evidence of symmetry than do the amplitude data, particularly at higher frequencies (probably because of the reduced amplitude at higher harmonics). However, Lienert and Bennett (1977) show by sensitivity studies that their inversion is controlled mainly by the phase of B_r and B_z at low frequency, but only by the B_z phase at high frequency. Considering the scatter in the B_z phase, the upper crust is probably not well resolved, but overall the data are well behaved and fit a one dimensional model reasonably well.

The data of Lienert (1979) are taken from eight profiles across the transmitter and show less symmetry and more scatter than Lienert and Bennett's (1977) one profile. As with other surveys, some indication of dimensionality or lateral source

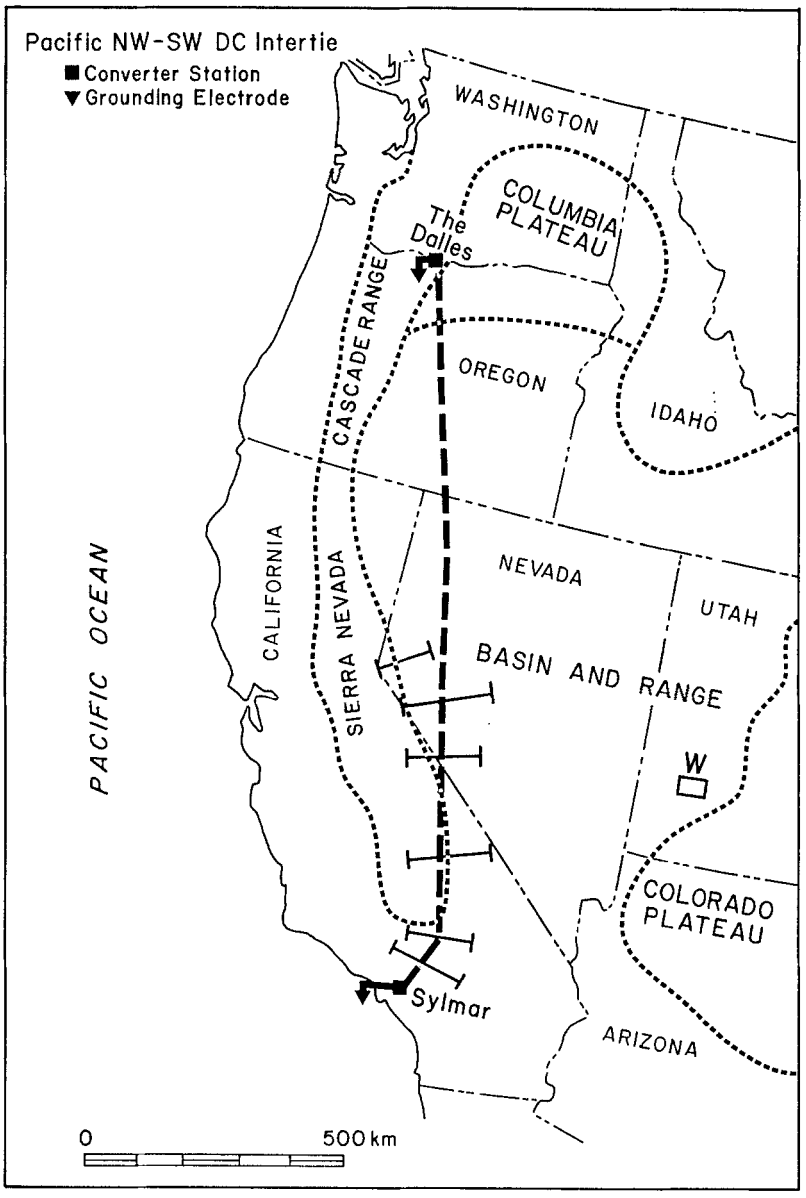

Fig. 14. A location map indicating the various CSEM and natural source experiments in the vicinity of the Pacific Northwest-Southwest DC power Intertie.

Fig. 15. An example of a profile published by Lienert (1977) which shows the amplitude and phase → of the horizontal and vertical magnetic fields from a power line source located at 0. The dotted line is the response of the preferred model (also illustrated).

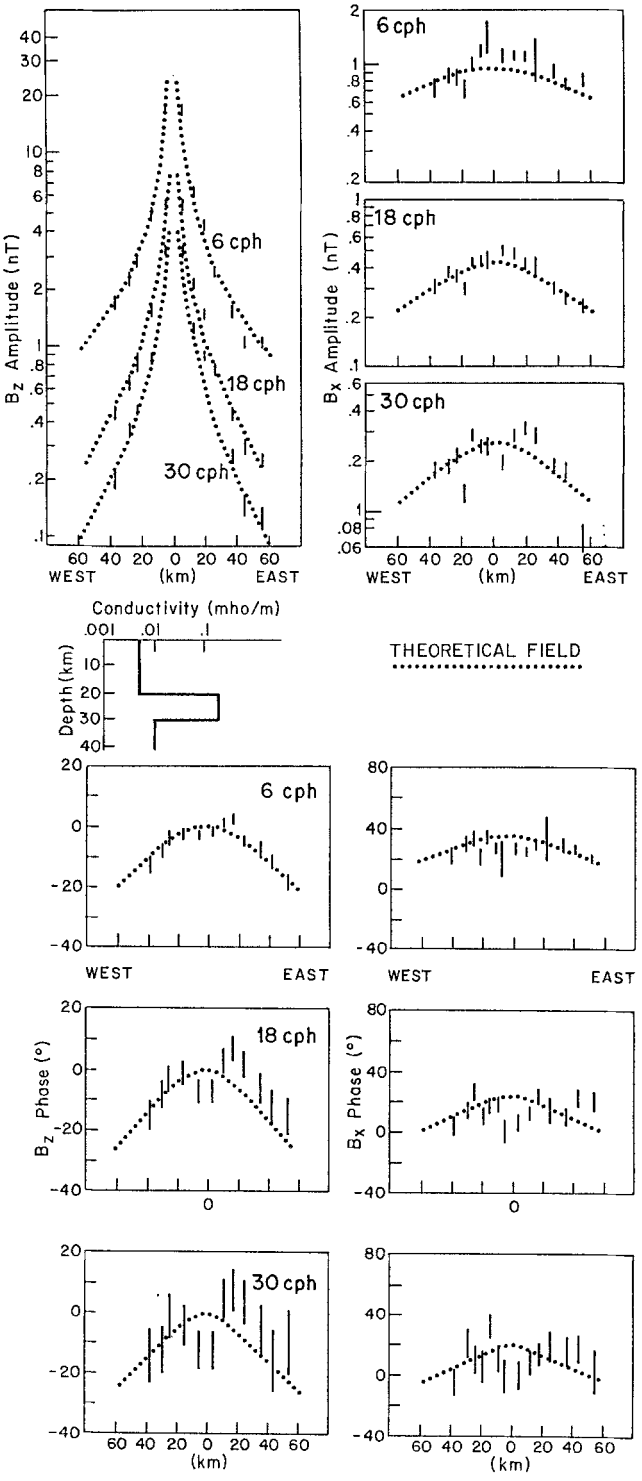
B_z Amplitude (nT)
6 cph
18 cph
30 cph
WEST
(km)
EAST
B_x Amplitude (nT)
Conductivity (mho/m)
.001 .01 .1
Depth (km)
10
20
30
40
THEORETICAL FIELD
B_z Phase (°)
B_x Phase (°)

effects could have been derived from magnetic fields parallel to the power line, but these were either not recorded or not reported. It is clear that most of the data are disturbed by the complicated geology in the region consisting of sediments, volcanics, intrusives and metamorphic rocks. One striking example is the effect of the Sierra Nevada batholith on the west side of the transmitter on profile line H-I which appears as a clear decrease in amplitude of the horizontal magnetic field over the resistive batholith. However, there are the common features in the data from all profiles which suggest a conductive feature at depth (or located laterally from the source).

Wannamaker (1983) finds no evidence for the deep conductor reported by Lienert and Bennett (1977) and Lienert (1979), but his MT data were collected on the eastern side of the Basin and Range province, a large distance from the receiver sites. Wannamaker (1983) did show that sedimentary basin fill in the province is highly conductive. Mackie *et al.* (1988) used MT data from the western side of the Sierra Nevada batholith and also find no evidence of high crustal conductivity to the east of the batholith. These data, however, are much more sensitive to the conductivity of the ocean and the oceanic mantle than the inland crust. Incidentally, the transverse resistance for the oceanic lower crust estimated by Mackie *et al.* (1988) is remarkably similar to that obtained by Cox *et al.* (1986) (i.e. between 2 and 5×10^9 Ω-m^2) in a novel seafloor CSEM experiment. Schmucker (1970) performed a geomagnetic depth sounding experiment to the north of Lienert and Bennett's (1977) profile and required a conductive feature at 40 km depth to explain the data, but the depth and conductivity of this feature are not well resolved.

Wannamaker (1983) suggested that the assumption of a 2D source by Lienert and Bennett (1977) and Lienert (1979) might not be appropriate because of Towle's (1980) experience with the same power line. Towle (1980) was conducting a geomagnetic depth sounding study near the power line when the positive side of the $\pm$400 V supply failed. The emergency grounding of the line and resulting current imbalance lasted several minutes before transmission in the line was finally halted. Towle (1980) interpreted the magnetic field from this nearly DC transmitter in terms of current channelling and found that some 50% of the transmitted current was returning along a path less than two kilometers from the line. This incredibly large amount of current is based on computing the difference between the theoretical DC magnetic field for a 1D earth and the actual measured field. However, the current used in the calculation of the primary field was the maximum rated current for transmission in the balanced line (1730 A at 1.4×10^9 W). An independent estimate of the current in the unbalanced line can be obtained from observations of H_z very close to the line, assuming the primary field is much stronger than the secondary field at this point. The data from a station 8 km from the line suggests that the current in the unbalanced line was actually 872 A, almost exactly 1/2 that used in Towle's calculation. When the primary fields are

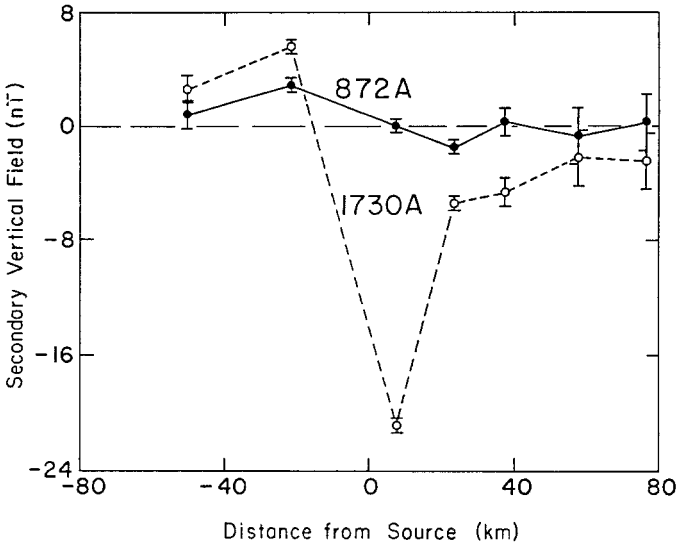

Fig. 16. Secondary vertical magnetic field amplitude at very low frequency from the 1400 km long Pacific Northwest-Southwest Intertie power line (see Figure 14). The dotted line is the field calculated from data given in Towle (1980) assuming a source current of 1730 A while the solid line is the secondary field computed assuming the secondary field at the closest station (8 km) is insignificant relative to the primary field. The observed field at 8 km from the source was approximately 21 nT which corresponds to a current of 872 A.

recalculated using this current, the secondary field at most sites is often within the quoted measurement error (see Figure 16) and so contingent on determining the actual current in the unbalanced line, there is little evidence of current channelling in Towle's data.

5.3. Data redundancy

There are essentially two, equally important, forms of data redundancy. Signal stacking and noise cancellation techniques can effectively reduce the requirements for large source moments by recovering low amplitude signals. However, if the earth is quasilayered, repeated spatial sampling can also be used to reduce noise and the response of structure too small to be resolved by the EM measurement. A very important advantage of controlled source experiments is that at large signal levels a high amount of data redundancy can be achieved without significant expense.

Spatial averaging has previously been applied to CSEM (e.g. Garg and Keller, 1986) but a particularly dramatic example of the method's effectiveness can be seen in the data from a large loop EM survey in the Kapuskasing uplift region in the Superior province of Northern Ontario. The Kapuskasing structural zone is interpreted as an exposure of high-grade metamorphic rocks along a Proterozoic thrust fault through the Archean crust. Two recent controlled source EM sound-

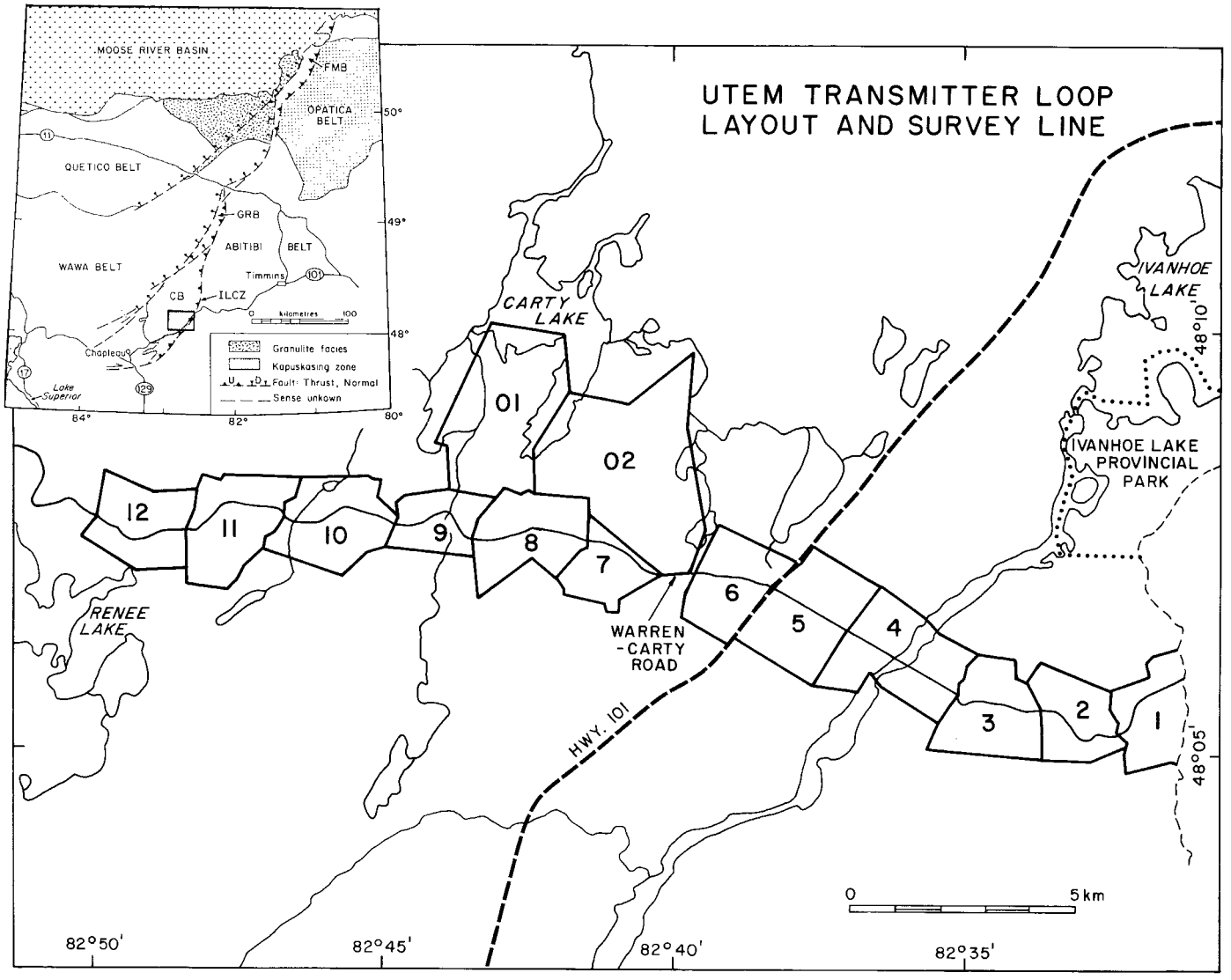
UTEM TRANSMITTER LOOP
LAYOUT AND SURVEY LINE
MOOSE RIVER BASIN
FMB
OPATICA BELT
QUETICO BELT
GRB
ABITIBI BELT
WAWA BELT
Timmins
CB
ILCZ
Chapleau
Lake Superior
Granulite facies
Kapuskasing zone
Fault: Thrust, Normal
Sense unkown
84°
82°
80°
50°
49°
48°
CARTY LAKE
01
02
12
11
10
9
8
7
6
5
4
3
2
1
RENEE LAKE
WARREN -CARTY ROAD
HWY. 101
IVANHOE LAKE
IVANHOE LAKE PROVINCIAL PARK
48°10'
48°05'
0
5 km
82°50'
82°45'
82°40'
82°35'

ings (Kurtz *et al.*, 1989; Bailey *et al.*, 1989) have been conducted over the region with the inductive source UTEM system (West *et al.*, 1984). The data consist of the step response vertical magnetic field from several loop sources which were on the order of 4–6 km^2 in area. Receiver profiles crossed through the loop and the largest offset from the center of the loop was on the order of 10 km. The current in the loop was only 1 A, giving a source moment of approximately 2.5×10^7 A-m^2. The Kapuskasing surveys are quite different from the other published inductive source deep sounding experiments because of the weak source moment. Also, measurements were made quite near the source, only the H_z component was observed and the lowest frequency attainable was the source waveform repetition frequency of 31 Hz.

There is tremendous redundancy in the combined data sets with 14 loop locations and several hundred receiver sites (Figure 17). Figure 18 shows a subset of the data as a set of profiles through transmitter loop 6 (Bailey *et al.*, 1989), where each profile line represents the average amplitude of H_z in a different time sample window. All data are presented as a normalized percentage of the measured primary field. The lack of symmetry about the source is immediately apparent, as is the rapid spatial variation of the early time data. On the western edge of the profile, the relatively smooth spatial variation at late time and at large distance from the loop edge is representative of a layered earth response. The near surface structure does not cause significant distortions in the late time data because the Fréchet derivative of the measurement to near surface structure is quite small (e.g. Figure 2, the step response sensitivity function).

The interpretation of the deep conductivity structure is based on Depth Image Processing (DIP, Macnae and Lamontagne, 1987) which essentially estimates the cumulative conductance based on the acceleration with depth of the induced current system. DIP apparently works well when the earth is quasi-layered and has the additional benefit of performing a certain amount of lateral smoothing. Although DIP may produce a depth-conductivity section which is similar to the actual structure, the procedure is not an inversion and there will always be some loss of fidelity from the original data. As with all depth-section displays, the DIP output is difficult to appraise in terms of the fit to the original data, data variance and data scatter.

The interpreted depth section, Figure 19, shows near surface structure and two layers embedded at two and five km depth in a very poorly conducting material (a gneiss, probably $<2 \times 10^{-5}$ S/m, but not well resolved by the data). The two deeper layers have slightly larger conductivities than the background, approximately 2×10^{-4} S/m. Forward modelling of the interpreted depth section shows

← Fig. 17. Locations of the source loops used in the Bailey *et al.*, 1989 and Kurtz *et al.*, 1989 UTEM surveys near the Kapuskasing structural zone.

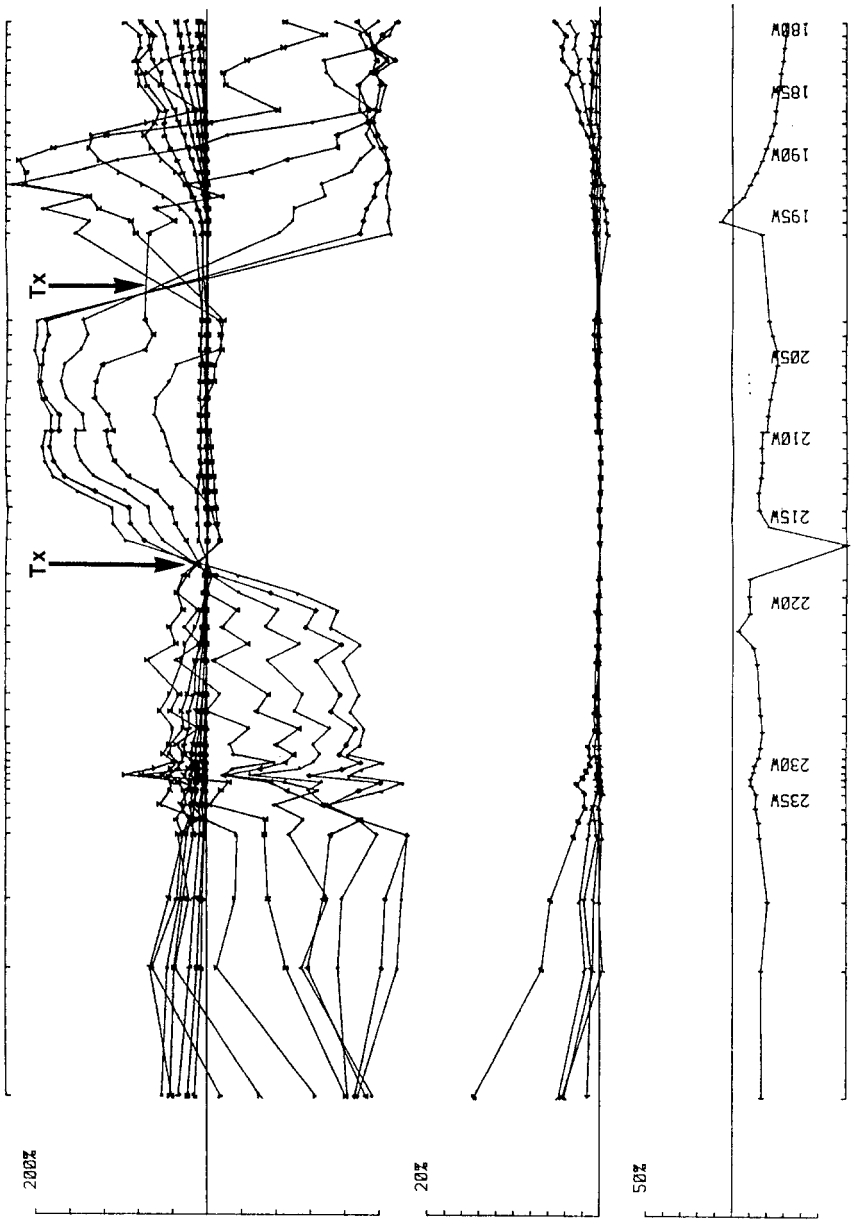
Tx
Tx
200%
20%
50%
180W
185W
190W
195W
205W
210W
215W
220W
230W
235W

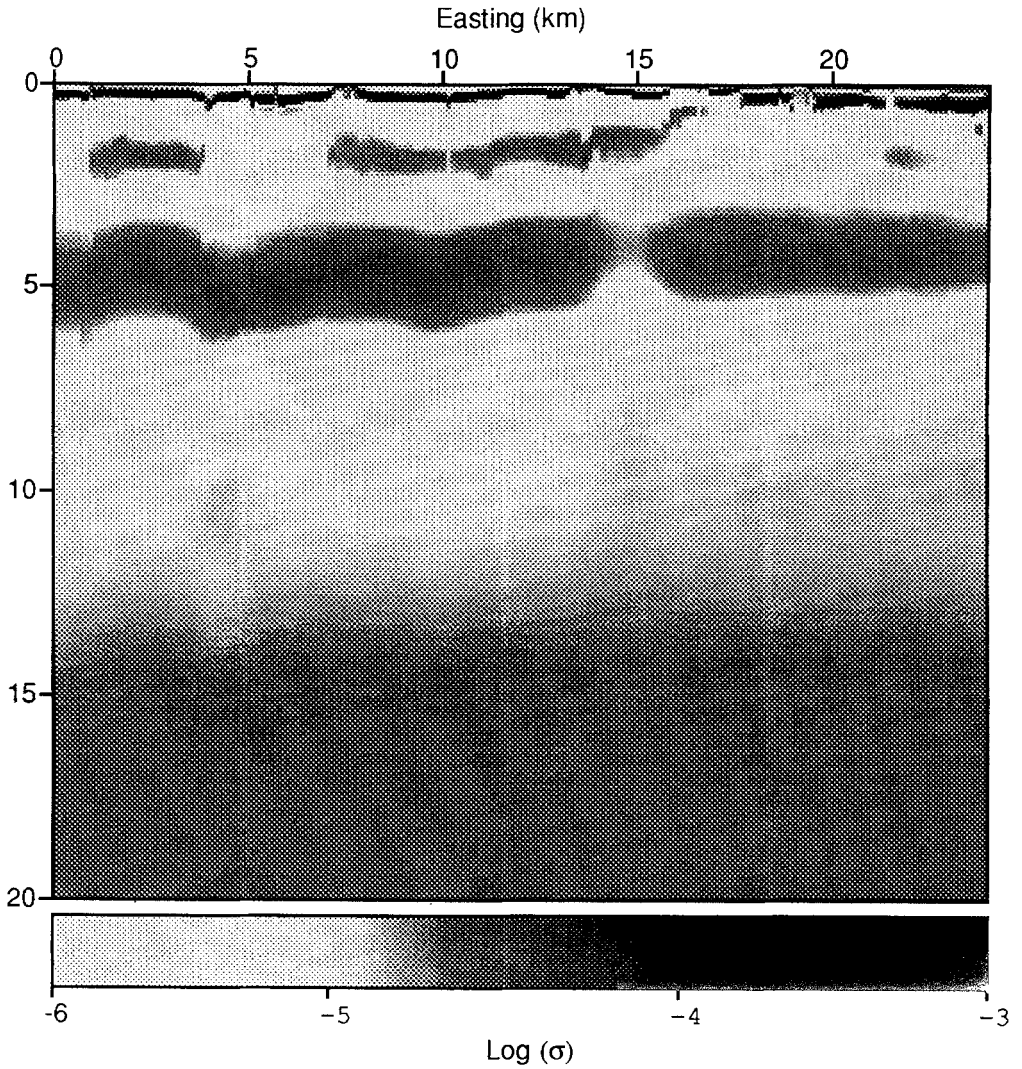

Fig. 19. The Depth Image Processing pseudo-section of interpreted conductivity versus depth. Aside from some surficial features there are two conductive layers at approximately 2 and 5 km. The general increase in conductivity with depth below 10 km is not well constrained (after Bailey *et al.*, 1989).

that for the parameters used in the UTEM surveys the difference in H_z between a background halfspace and a model containing the interpreted conducting layers is of the order of five to ten percent (but is strongly dependent of source/receiver offset). The variability in the data because of near surface conductors (mostly clays) is sometimes an order of magnitude larger the response from the layers (see Figure 18). Without several hundred measurements over a wide time band, the common features of a conductive layer at depth would have been difficult to

interpret with any certainty. Inversion of a selected subset of the data agrees quite well with the DIP interpretation (Bailey *et al.*, 1989).

The natural source data collected in the area (geomagnetic depth sounding (GDS): Woods and Allard, 1986, MT: Kurtz *et al.*, in preparation) indicated that the electrical structure of the middle and upper crust was relatively uniform laterally along a 100 km long profile. Much of the data are distorted by surficial features, but the average conductivity of this part of the crust was estimated at 2.5×10^{-5} S/m. An increase in conductivity starting about 12 km is detected in the MT data and there is a hint of this also in the UTEM data. However, the agreement between the cumulative conductance estimates determined by each method is excellent for the middle and upper crust, although neither technique has the facility for resolving the conductivity of the host.

5.4. Modal contributions

A very important difference between natural source methods and CSEM for a layered earth investigations is that TM mode current flows can be generated by artificial sources. Since the TM mode is sensitive to the charge on conductivity gradients it is possible to resolve resistive as well as conductive layers. Joint interpretations of data from different experiments which individually yield the TM mode and PM modes have occurred quite often in the literature (e.g. Vozoff and Jupp, 1975; Drews *et al.*, 1989; Hördt, 1989). A less common application of this enhanced interpretation method is to generate both modes with a grounded bipole source and measure all components of the EM fields (which ensures sensitivity to both PM and TM modes of current flow). Many sounding experiments have employed grounded bipole sources, either as DC resistivity sources or in a mode called Long Offset Transient EM (LOTEM, e.g. Keller *et al.*, 1984; Strack, 1984; Strack *et al.*, 1989b). While there are many variations on the basic LOTEM configuration, the most common sounding technique is to observe the vertical magnetic field (PM mode only). More recently, measurements of the electric field have been made as well. The vertical magnetic field method of sounding can be very effective where the earth is quasi-layered and if 1D conductive targets are of interest (see Gunderson *et al.*, 1986 for examples of 3D responses). However, when it is important to detect the resistive features, or to understand 3D scattering, incorporating the horizontal electric and magnetic fields into the interpretation can result in significant improvements in resolution. Two excellent examples of the resolution improvement by incorporating electric field data in a 1D inversion were reported by Strack *et al.* (1989b) and Vozoff *et al.* (1985), albeit for relatively shallow studies (i.e. $\approx$2 km).

The first example, Strack *et al.* (1989b), was from a producing oilfield in western Europe where seismic reflection data indicated the geological strata were predominantly horizontal. Layered earth inversions were used to show that the magnetic field data were sensitive to the depth of the resistive layer at 2 km, but only

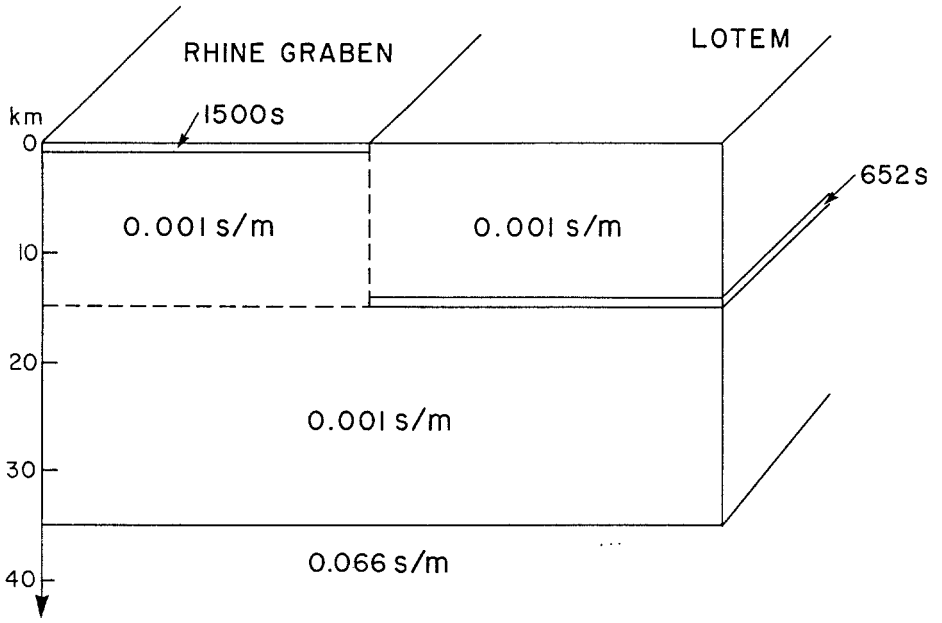

Fig. 20. A model derived from MT measurements near the Rhinegraben (indicated by a high surficial conductance. The conductive layer at a depth of almost 15 km on the east side of the Rhinegraben is below the region of LOTEM soundings. The upper crustal conductivity above the conductive layer is approximately 0.001 S/m (after Wilhelm *et al.*, 1989).

by incorporating the electric field data was it possible to resolve the conductivity (4×10^{-3} S/m) and thickness of the layer. It was also demonstrated that relocating the source did not affect the interpretation, verifying the assumption of one dimensionality. In the second example (Vozoff *et al.*, 1985), the authors showed that electric fields could be used to constrain the conductivity of a carbonate layer, the depth of which had been determined by seismic reflection and drilling. The significant achievement of this survey was in mapping the lateral change in porosity of this hydrocarbon reservoir.

LOTEM has also been used for deep crustal studies (e.g. Strack *et al.*, 1990; de Beer *et al.*, 1991; Skokan and Anderson, 1991), but usually only for PM mode measurements. MT and LOTEM measurements were made in the Black Forest as a component of the multidisciplinary studies for the selection of the drill site for the German Continental Deep Drilling Program (KTB: Kontinentales TiefBohrprogramm; Wilhelm *et al.*, 1989). A schematic of the 2D interpretation from the MT data is given in Figure 20 which shows a conductive zone at a depth of approximately 15 km on the eastern side of the Rhinegraben where the LOTEM survey was carried out. The MT data (and GDS data) showed pronounced indications of multi-dimensional EM responses, but the spatially confined LOTEM source fields were certainly less affected by the conductive sedimentary fill of the

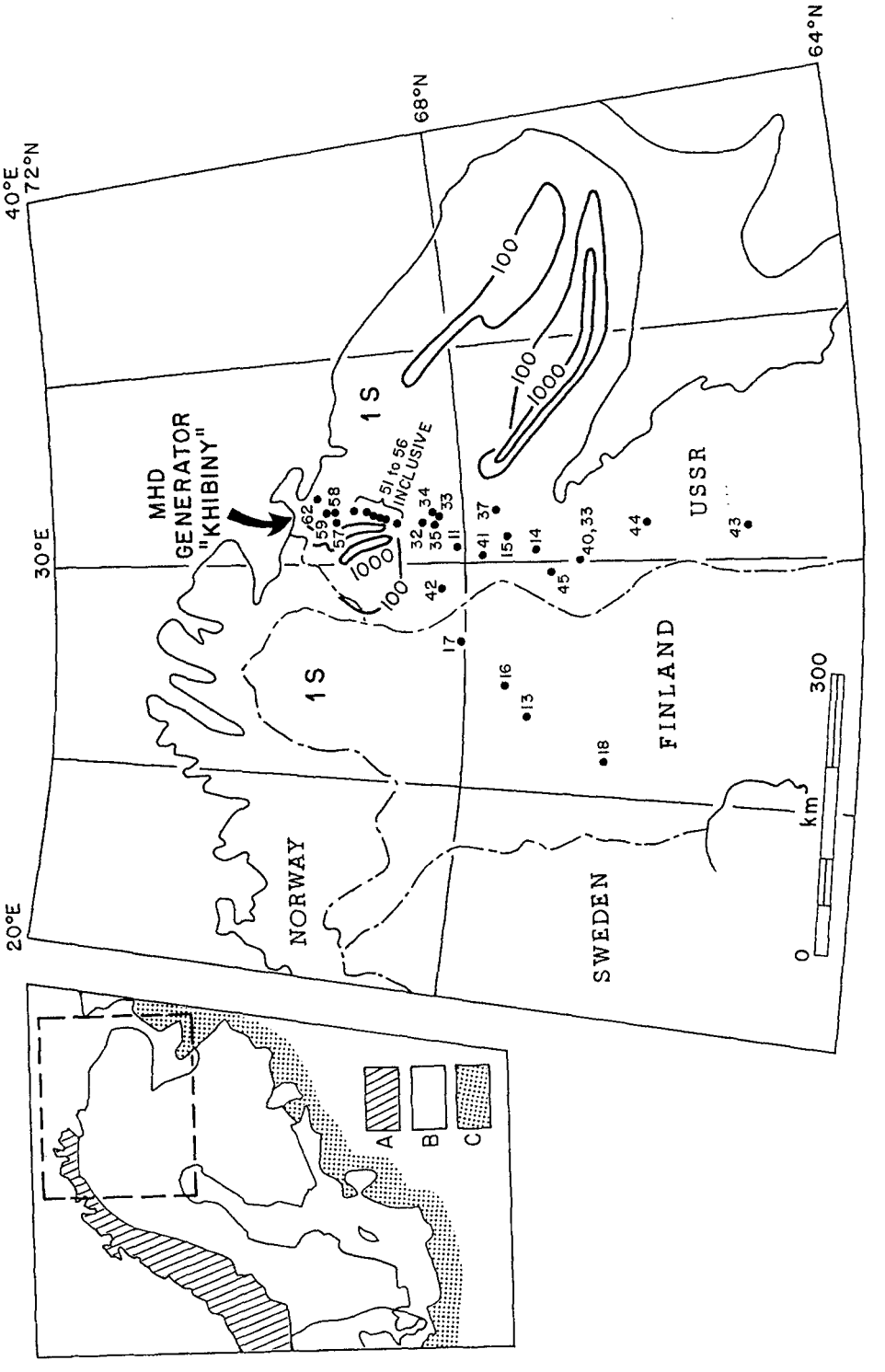
40°E
72°N
68°N
64°N
30°E
20°E
MHD
GENERATOR
"KHIBINY"
1 S
1 S
1 S
51 to 56
INCLUSIVE
100
1000
100
100
1000
100
NORWAY
SWEDEN
FINLAND
USSR
0
300
km
A
B
C

Rhinegraben. However, while the LOTEM and MT/GDS interpretations both detect conductive zones at depth, there is some discrepancy between the preferred models from each technique. One dimensional inversions of the LOTEM data at multiple stations and from two different transmitter locations indicate a laterally uniform upper crust with a zone of enhanced conductivity at depths of 7–9 km, at last 500 m thick. Wilhelm *et al.* (1989) suggest that since the shortest period MT data is at 10 s, it is possible that the zone detected by CSEM experiment was not resolvable in the MT. An alternative explanation suggested by Jones (1991) is that the MT data are "static shifted" (e.g. Jones, 1988). The MT model consists of 0.001 S/m layer overlying a 0.1 S/m layer at a depth of 12 km, whereas the LOTEM results indicate that the uppermost part of the crust is some 0.0025 S/m with a conducting zone of some 0.25 S/m (Strack *et al.*, 1990). Assuming that the upper crustal conductivity should be the same for the two models, the MT data should be shifted by a factor $\sqrt{2.5}$ which gives a depth (for a 1D model) of some 7.5 km or the top of the conducting zone. This depth agrees with the LOTEM results and also correlates spatially with a pronounced low velocity layer between depths of 7–14 km, above a laminated lower crust (Wilhelm *et al.*, 1989; Strack *et al.*, 1990).

5.5. Near source effects

Very interesting and instructive examples of deep controlled source soundings are experiments with the MHD generating station "Khibiny" located on the Kola peninsula (Velikhov *et al.*, 1986). A sketch of the coastal topology and source geometry is shown in Figure 21. The source is notable not only for the tremendous output power and large distances at which the fields can be detected for ultra deep sounding, but also for the location on the coast. The source bipole is grounded into the sea bed on either side of the Sredny Peninsula which results in such a low contact resistance that the system is capable of generating some 22 000 A of current. A typical current pulse is almost rectangular in shape and has a duration of five to seven seconds. In general, all five components of the EM fields were recorded at remote receiver sites with radio synchronization for relative timing control.

The MHD source configuration presents some theoretical difficulties because much of the current in the system will find an almost horizontal return path through the sea water and only a fraction of the current will penetrate the earth through the grounding points. Dyakonova *et al.* (1983) used a layered earth conductivity structure determined from magnetotelluric soundings and were able to model the geometric decay of the low frequency electric fields from the MHD

← Fig. 21. Geographic location of the Khibiny magnetohydrodynamic (MHD) generating station. The labeled points are receiver locations which were used in the interpretation by Vanyan *et al.* (1989).

generator out to 400 km by representing the MHD sources as a grounded dipole source. The calculated magnetic field response of this model, however, was much lower in amplitude than the measured response. In fact, Dyakonova *et al.* (1983) found that the response of the proposed model was much closer to the data when the source was represented by distributing the current between superimposed electric (20%) and magnetic (80%) dipoles. The center of the effective VMD was determined to be just north of the Ribatchy peninsula (Figure 22). This study illustrates how the deleterious effects of near surface conductors could be addressed by determining an equivalent source distribution. The fields from this equivalent source can then be used for interpretation of deep structures without resorting to complicated models of the near surface.

The difficulties inherent in modelling the Khibiny MHD source are apparent in that most of the interpretation is based on the DC electric fields. Velikhov *et al.* (1986) present low-frequency isoline maps of the total electric field amplitude and the vertical and horizontal magnetic field components (Figure 22). These maps should be an essential first step in interpretation for they clearly define major crustal blocks and anomalous zones of conductivity (e.g. the graphitic Pechenga and Varzuga zones). Although the absolute levels of apparent conductivity or conductance defined by the data are in question because of the complicated coastal effect, the relative changes in the data are still important for defining lateral structure.

Vanyan *et al.* (1987, 1989), and Kaikkonen *et al.* (1988) model the Baltic shield as a thin resistive sheet (defined by transverse resistance) adjacent to the conductive Barents sea (defined by conductance). Below the thin sheet, the model consisted of a resistive upper crust and an infinitely conductive basement. These studies were meant to address the effect of near surface heterogeneity near a CSEM transmitter, and the subsequent resolution of layered earth structures beneath the laterally inhomogeneous thin sheet. The data consist of apparent conductivity defined from the modulus of the total electric field, a definition which ignores any directional information. Vanyan *et al.* (1989) found that by including the conductive Pechenga and Varzuga graphite zones in the model, a remarkably good fit to the data could be obtained up to 200 km from the source. Beyond 200 km, the data are scattered enough that the apparent conductivity curve could turn up, signifying the conductive base to the crust, or continue to decrease providing no evidence of deep conductivity (Figure 23). The profile which extends

Fig. 22. Figure (a) shows the isolines of $|E|$ in mV/km at low frequency, the orientation of the electric → field vector (solid arrows) and the orientation of the horizontal magnetic field vector (dashed arrows) for the Khibiny MHD source. Note that **E** and $\mathbf{H}_{\text{Horizontal}}$ are rarely orthogonal. Figure (b) shows vertical magnetic field isolines (solid lines) and the magnitude of the horizontal magnetic field (dotted lines). The estimated configuration of the magnetic dipole part of the MHD source currents is sketched in the northern part of the Ribatchy peninsula as a set of flow lines (from Velikhov *et al.*, 1986).

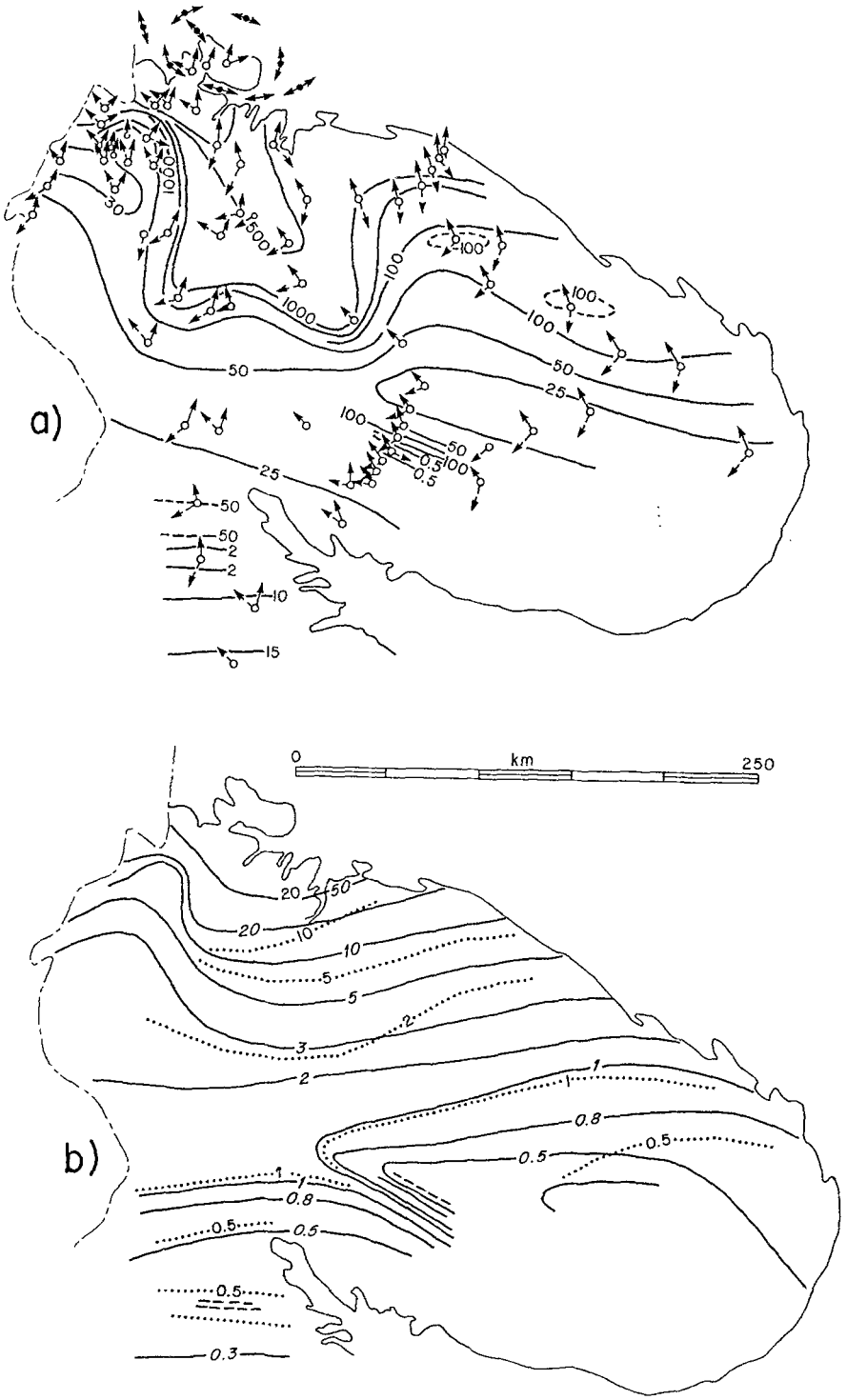
a)
1000
500
100
30
1000
100
100
100
100
50
50
25
25
100
50
0.5
100
0.5
50
50
2
2
10
15
0
km
250
b)
20
50
20
10
10
5
5
2
3
2
1
1
0.8
0.5
0.5
1
1
0.8
0.5
0.5
0.5
0.3

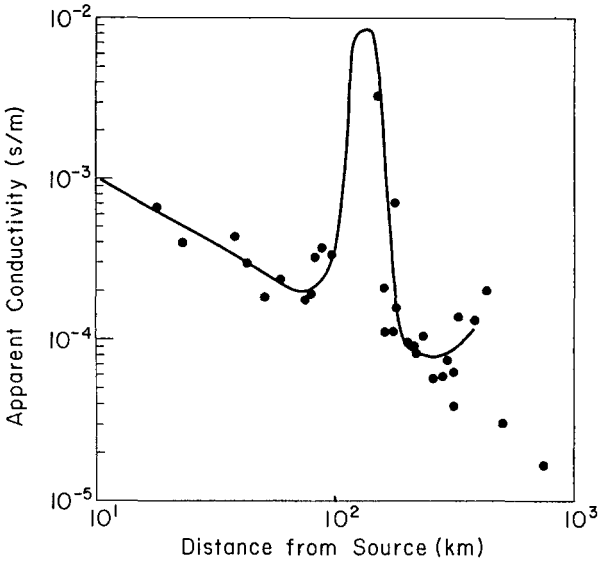

Fig. 23. A conductivity profile devised by Vanyan *et al.* (1989) based on the amplitude of the total electric field vector at each measurement site. The huge increase in conductivity before 200 km is due to a conductive graphite zone, but the general trend is to an increasingly more resistive crust with depth. The solid line is the response of an inhomogeneous thin sheet model overlying a layered earth. The increase in conductivity at long periods is supported by the profile into Finland (see Figure 17).

into Finland seems to support the deep conductor model. Vanyan *et al.* (1989) show that the resistance of the upper layer correlates well with that determined by magnetotellurics, although the MT average apparent conductivity is very small (poorly resolved ?) at $\approx 4 \times 10^{-6}$ S/m.

5.6. Apparent conductivity

Apparent conductivity is a very useful indicator of trends and levels in the data and can remove some of the effect of the transmitter/receiver configuration. Apparent conductivities do contain certain artifacts, even for 1D models, and are probably better defined as a tensor for CSEM surveys in which multiple components of the EM field are recorded (e.g. Bibby, 1986). The physical meaning of apparent conductivity can become quite complicated for data collected in complex geological environments. Caution should always be used in assigning an interpretation to apparent conductivity.

One example of complications arising from trying to interpret apparent conductivity is contained in the work by Heikka *et al.* (1984) who conducted a deep sounding experiment at two receiver sites in Finland using the fields from the Khibiny MHD station. The authors make the perplexing observation that a site at 193 km from the transmitter (Ivalo) is in the far-field of the source while a co-linear site at 333 km (Sodankylä) is not (Figure 24). This conclusion is based on

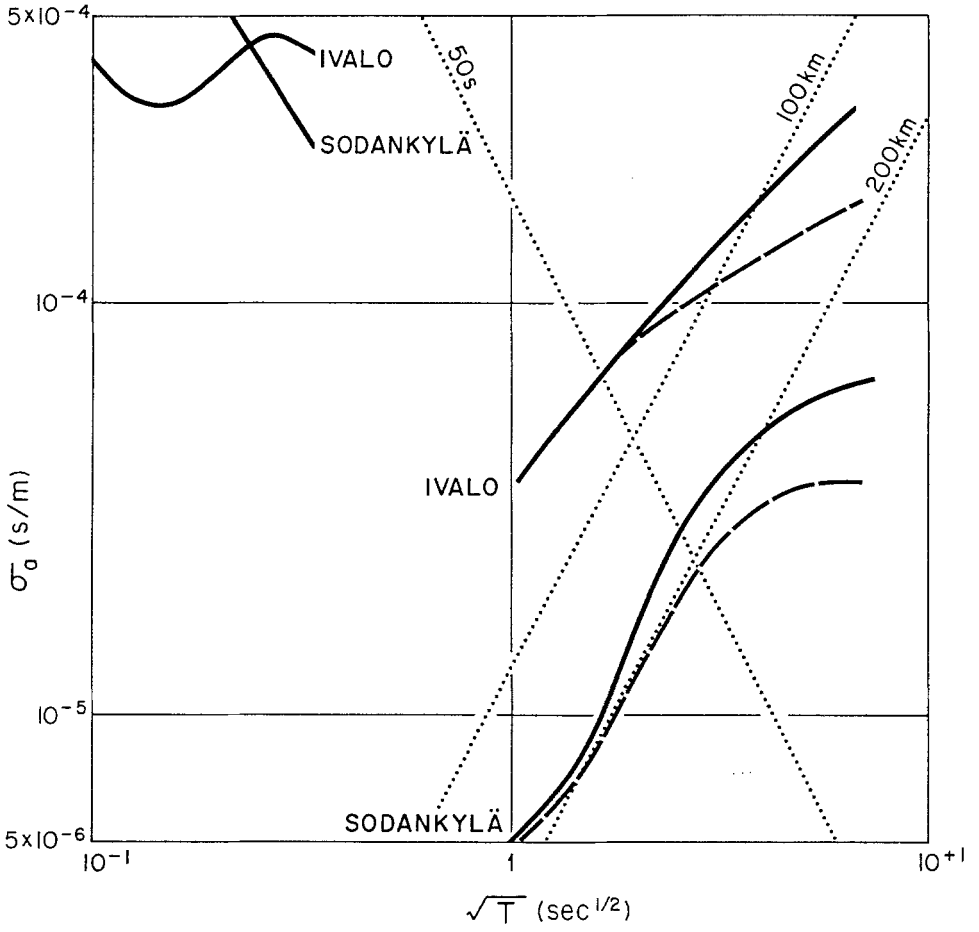

Fig. 24. The interpreted apparent conductivity curves as a function of the square root of period for the MHD soundings in Finland (after Heikka *et al.*, 1984). The solid curves are computed from the full definition of the electric field on a halfspace, while the dashed curves are computed from the far-field limits of these expressions. Also indicated are diagonal lines showing the depths to a perfect conductor, and the conductance as a function of period. The shorter period AMT data at the same sites is shown on the left of the plot.

comparison of two apparent conductivity estimates at each site; one computed from the far-field limit of the electric field on a halfspace, and the other computed from the general expression for the electric field on a halfspace. When these two calculations yield a consistent apparent conductivity the authors maintain the data were recorded in the far-field. Data which were deemed far-field were subsequently interpreted in terms of plane wave models, making testing of the far-field conditions a crucial stage in the interpretation.

It is an admittedly difficult task to decide when data are recorded in the far-field of a source for complicated geological environments since the scattered fields

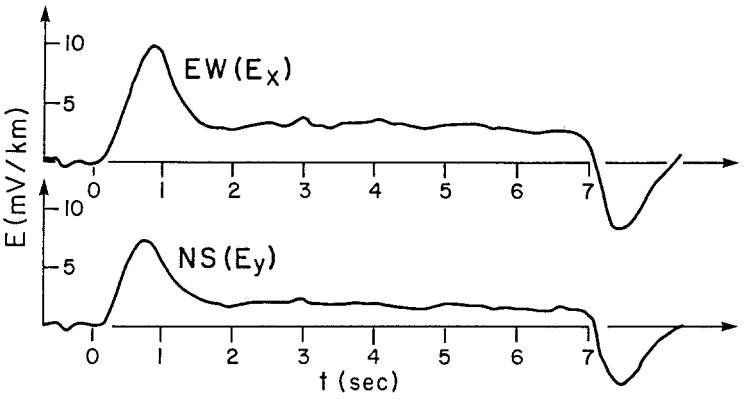

Fig. 25. Examples of the measured electric field at Sodankylä from the MHD generator at the Khibiny station. The low frequency amplitude of the total electric field is approximately 4 mV/km (from Heikka *et al.*, 1984). Using this value in the apparent conductivity formulas leads to an order of magnitude increase in conductivity at the Sodankylä site compared with that presented in the previous figure.

can be expected to have significant wavenumber components. One particular problem with comparing two apparent conductivities based on the electric fields is that these quantities can be highly biased by local conductivity structures. Measurements made on a small, but highly resistive feature will result in a small apparent conductivity which may not be appropriate for describing the regional characteristics of the EM fields. Sodankylä is located near the central Lapland granite massive and the Ivalo site is on the conductive northern portion of a granulite belt. Using the calculated apparent conductivities, at Sodankylä $|\gamma_a r| = 2.1$, whereas at Ivalo $|\gamma_a r| = 3.8$ at 1 Hz. If the reported apparent conductivities are representative of the crust, Ivalo is much closer to meeting the far field condition than Sodankylä. However, the large difference between the two values of σ_a suggests strong 3D scattering, making the interpretation of the apparent conductivities much more complicated than the 1D case.

In fact, the 3D effects in the data of Heikka *et al.* (1984) may not be as severe as indicated in the paper. Figure 25 (taken from Heikka *et al.*, 1984) shows that the magnitude of the electric field recorded at Sodankylä is approximately 4×10^{-6} V/m. They also give the source/receiver separation as $r = 333$ km and source moment as $Idl = 3.5 \times 10^7$ A/m. Using these values, the apparent conductivity calculated for the Sodankylä site at 1 Hz is approximately 5×10^{-5} S/m, a factor of ten larger than reported by Heikka *et al.* (1984). In this case, the interpretation of an average crustal conductivity is consistent between Ivalo and Sodankylä and there is a much improved correlation between the CSEM interpretation and the reported natural source AMT data.

If these conductivities are a reasonable average for the Baltic shield, the authors' contention that the measurements at Sodankylä are in the far-field is more realistic ($|\gamma_a r| = 6.6$), although the reported depth of investigation is dramatically reduced

from approximately 175 km to less than 100 km. A larger number of stations would have helped considerably in determining an average conductivity for the region to decide if the source fields have plane-wave characteristics. It may be better to use 1D models with 3D surficial structure and 3D sources (following Vanyan *et al.*, 1989) than resort to plane wave calculations for 2D and 3D models without some a priori justification. If there is some spatial variation in the data which is due to the source field, this response may be interpreted as geological structure using plane wave modelling algorithms because of the duality between sources and boundary conditions.

6. Discussion

The 1D theory of deep sounding, controlled source EM methods can be generalized to emphasize the similarities of the many practical methods. As a result of this redundancy there are many possible methods for sounding a one dimensional earth. As well, it may not be necessary to have measurements of all field components from these sounding experiments because this also represents a substantial and operationally expensive redundancy. However, perhaps the greatest restriction to applying controlled source methods for deep sounding is the limited modelling capabilities. This deficiency impacts on experimental design, data acquisition, interpretation and resolution analysis. In light of this fact, it would be prudent to acquire as much information about the CSEM field as possible and prove that the expected redundancy and interrelations between field components exist. If this can be done, no criticism can be leveled at the experiment for improper modelling. It is also critically important to know when the data do not warrant 1D interpretations and to seek out alternative methods of interpretation.

There are a number of apparent biases in published deep CSEM work which should be considered when appraising the results of a particular survey. The first bias is simply in the selection of sounding locations. Site location can be chosen by convenience or because of the fortuitous availability of some EM source. Archean regions are also favored because of the generally low conductivity permitting deep penetration of the EM fields with little attenuation. However, the low surface conductivity also allows the EM fields to expand laterally over significant distances to interact with surficial structures.

Another prominent bias in deep sounding is that most experiments can be classified as being sensitive to either TM mode or PM mode measurements, but not both. This is perhaps unfortunate because the optimal resolution of $\sigma(z)$ can only be obtained through interpretation of data from both modes. Deep DC resistivity sounding reveals the upper crust as containing complicated surficial structures (usually sedimentary), but the middle crust is highly resistive and may be underlain by conductive material. Inductive soundings provide a similar picture of the crust and provide more evidence for a deep conductive layer (see Jones,

1991), but fail to constrain the transverse resistance of the upper crust. The presence of a conductive layer in the deep crust can be challenged to some extent in most of these data, but cannot be discounted.

Since CSEM interpretations are mostly limited to a single dimension, whether it is sufficient to interpret only one of the PM or TM modes must be addressed. The PM mode is sensitive to high conductivity but cannot be used to resolve the more resistive portions of the section, and the TM mode is sensitive to both high and low conductivity, but can be easily "screened" from deep layers by overlying resistive layers. To a large extent, the information provided by the two modes is complimentary and assigning the response of only one mode to fit EM data from complicated environments is of dubious value.

Both PM and TM modes are necessary to resolve transverse isotropy ($\sigma_h \neq \sigma_v$). Anisotropy is an under-used concept in EM sounding since it can represent the aggregate response of a very complicated media without excessive computational resources. An example of how transverse isotropy might prove useful is in describing the "layered reflectors" observed in regional seismic reflection studies throughout the world. EM methods have little hope of resolving this fine structure at the same scale as seismic reflection methods, but determining if these zones are electrically anisotropic could put strong constraints on the interpretation of such features. Since transverse isotropy does not affect the PM mode and simply scales depths in the DC TM mode, independent inversion of either mode will produce biases in interpretation, even for perfect data on an anisotropic layered earth. Both modes must be observed over a large frequency (or time) bandwidth and inverted simultaneously to resolve any information about anisotropy in a 1D earth. Incorporating anisotropy is also a useful manner of permitting rapid variations in small scale structure which would otherwise be obviated by regularization ("least structure models") in inversion programs (e.g. Constable *et al.*, 1987; deGroot-Hedlin and Constable, 1990).

The final bias of many CSEM experiments is that only certain components of the EM fields are recorded. On a 1D earth, this approach can be quite adequate for a robust and reliable interpretation of the conductivity profile while resulting in lower acquisition time and reduced field costs. There is no doubt that the real world is 3D and the EM response of the earth will always be more complicated than numerical or scale modelling suggests. Throughout this review it has been emphasized that measurements of all components of the EM fields might validate the choice of a simplified model during interpretation. Moreover, the auxiliary information can be beneficial for interpretation when the EM response is more complicated than expected. Field components which are independent of a 1D conductivity structure could, at the very least, be used as "dimensionality indicators". These anomalous components should be very desirable quantities to use for interpreting 3D structure since they are a direct measure of the 3D scattered fields in the earth. Such components could be mapped to estimate the location of

the scattering body since the problem of separating the 1D and 3D responses is trivial.

This review has hopefully illustrate some of the advantages and limitations of CSEM surveys. There is little doubt that deep EM sounding must involve some type of CSEM experiment for independent control when interpreting natural source data, or to gain additional information about the deep crust. For example, the presence of transverse isotropy in the crust can not be resolved by natural source measurements alone. In general though, CSEM should act as a compliment to natural source studies. Numerical modelling will continue to be a source of difficulties for CSEM interpretation although as modelling capabilities improve, CSEM methods will only become more appealing for deep sounding.

> To doubt everything or to believe everything are two equally convenient solutions; they both dispense with the necessity of reflection. (H. Poincaré)

Acknowledgements

Many of the ideas presented in this paper were strongly influenced by my co-workers and I would like to acknowledge the many long discussions I have enjoyed the pleasure of with Jim Craven, Ross Groom, Alan Jones and Ron Kurtz. I also would like thank all my colleagues who kindly took time out from their busy schedules to respond to a circular canvassing for reprints and preprints of controlled source related work. This review would not have been possible without their cooperation. Although a great number of people have in some way contributed to this paper, I take full responsibility for any regrettable omissions or errors.

This is Geological Survey of Canada contribution number 16891.

References

Anderson, L. A. and Keller, G. V.: 1966, 'Experimental Deep Resistivity Probes in Central and Eastern United States', *Geophysics* **31**, 1105–1133.

Asten, M. W.: 1987, 'Full Transmitter Waveform Transient Electromagnetic Modeling and Inversion over Coal Measures', *Geophysics* **52**, 279–288.

Astrakhanstev, G. V., D'Yakonov, B. P., Bulashevich, Yu. P., Volkov, Yu. M., Ulitin, R. V., Titlinov, V. S., Kuksa, Yu. I., Bobrovnikov, N. V., Skachkov, P. P., Khachay, O. A., Krasnobaeva, A. G. and Vishnev, V. S.: 1979, 'Investigation of the Conductivity of the Crust in the Urals', *Izvestiya, Earth Physics* **15**, 56–64.

Bailey, R. C., Craven J. A., Macnae, J. C. and Polzer, B. D.: 1989, 'Imaging of Deep Fluids in Archean Crust', *Nature* **340**, 136–138.

Berdichevsky, M. N., Vanyan, L. L. and Fainberg, E. B.: 1969, 'Magnetovariational Sounding Using Spatial Derivatives of the Field', *Geomagn. Aeron.* **9**, 369–371.

Bibby, H. M.: 1986, 'Analysis of Multiple-Source Bipole-Quadripole Resistivity Surveys Using the Apparent Resistivity Tensor', *Geophysics* **51**, 972–983.

Blohm, E. K., Worzyk, P. and Scriba, H.: 1977, 'Geoelectric Deep Soundings in Southern Africa Using the Cabora Bassa Power Line', *J. Geophysics* **43**, 665–679.

Boerner, D. E. and West, G. F.: 1989a, 'A Generalized Representation of the Electromagnetic Fields in a Layered Earth', *Geophysical Journal* **97**, 529–548.

Boerner, D. E. and West, G. F.: 1989b, 'A Spatial and Spectral Analysis of the Electromagnetic Sensitivity in a Layered Earth', *Geophysical Journal* **98**, 11–21.

Boerner, D. E. and West, G. F.: 1989c, 'Fréchet Derivatives and Single Scattering Theory', *Geophysical Journal* **98**, 385–390.

Boerner, D. E. and Holladay, J. S.: 1990, 'Approximate Fréchet Derivatives in Inductive Electromagnetic Soundings', *Geophysics* **55**, 1589–1595.

Cantwell, T., Galbraith, J. R. and Nelson, P.: 1964, 'Deep Resistivity Results from New York and Virginia', *J. Geophys. Res.* **69**, 4367–4376.

Chave, A. D. and Cox, C. S.: 1982, 'Controlled Electromagnetic Sources for Measuring Electrical Conductivity Beneath the Oceans 1. Forward Problem and Model Study', *J. Geophys. Res.* **87**, 5327–5338.

Chave, A. D.: 1984, 'The Fréchet Derivatives of Electromagnetic Induction', *J. Geophys. Res.* **89**, 3373–3380.

Chave, A. D. and Booker, J. R.: 1987, 'Electromagnetic Induction Studies', *Rev. of Geophysics* **25**, 989–1003.

Connerney, J. E. P. and Kuckes, A. F.: 1980, 'Gradient Analysis of Geomagnetic Fluctuations in the Adirondacks', *J. Geophys. Res.* **85**, 2615–2624.

Connerney, J. E. P., Nekut, A. and Kuckes A. F.: 1980, 'Deep Crustal Electrical Conductivity in the Adirondacks', *J. Geophys. Res.* **85**, 2603–2614.

Constable, S. C.: 1985, 'Resistivity Studies over the Flinders Conductivity Anomaly, South Australia', *Geophys. J. R. astr. Soc.* **83**, 775–786.

Constable, S. C., McElhinny, M. W. and McFadden, P. L.: 1984, 'Deep Schlumberger Sounding and the Crustal Resistivity Structure of Central Australia', *Geophys. J. R. astr. Soc.* **79**, 893–910.

Constable, S. C., Parker, R. L. and Constable, C. G.: 1987, 'Occam's Inversion: A Practical Algorithm for Generating Smooth Models from EM Sounding Data', *Geophysics* **52**, 289–300.

Cox, C. S., Constable, S. C., Chave, A. D. and Webb, S. C.: 1986, 'Controlled Source Electromagnetic Sounding of the Oceanic Lithosphere', *Nature* **320**, 52–54.

de Beer, J. H., Le Roux, C. L., Hanstein, T. and Strack, K.-M.: 1991, 'DC Resistivity and LOTEM Model for the Deep Structure of the Northern Edge of the Kaapvall Craton, South Africa', *Physics of the Earth and Planetary Interiors* **66**, 51–61.

deGroot-Hedlin, C. and Constable, S.: 1990, 'Occam's Inversion to Generate Smooth Two-Dimensional Models from Magnetotelluric Data', *Geophysics* **55**, 1613–1624.

Drews, C., Fürch, N., Maurer, H. M., Musmann, G. and Weidelt, P.: 1989, 'Active Audiomagnetotellurics on Milos (Greece) for Determination of Electrical Conductivity Distribution and its Correlation with Geothermal Anomalies', *Geothermics* **18**, 507–519.

Duncan, P. M., Hwang, A., Edwards, R. N., Bailey, R. C. and Garland, G. D.: 1980, 'The Development and Applications of a Wide-Band Electromagnetic Sounding System Using a Pseudo-Noise Source', *Geophysics* **45**, 1276–1296.

Dyakonova, A. G., Dyaknonov, B. P. and Skachov, P. P.: 1983, 'Electromagnetic Survey Results of the Murmansk Block of the Baltic Shield: The Development of the Deep Geoelectric Model of the Baltic Shield', *Proceedings of the First Project Symposium*, Department of Geophysics, University of Oulu, Report No. 8, pp. 217–233.

Eaton, P. A. and Hohmann, G. W.: 1989, 'A Rapid Inversion Technique for Transient Electromagnetic Soundings', *Phys. Earth Planet. Interiors* **53**, 528–538.

Edwards, R. N.: 1975, 'The Magnetometric Resistivity (MMR) Method', Paper Presented at AIME Annual Meeting, February 17 in New York, reprint no. 75-L-82.

Esparza, F. J. and Gómez-Treviño, E.: 1987, 'Electromagnetic Sounding in the Resistive Limit and the Backus–Gilbert Method for Estimating Averages', *Geoexploration* **24**, 441–454.

Fiskina, M. V., Zinger, V. Sh., and Faynberg, E. B.: 1986, 'Applications of the Method of Space Derivatives in Deep Electromagnetic Studies with Controlled Field Sources', *Izvestiya, Earth Physics* **22**, 995–998.

Fullagar, P. K. and Oldenburg, D. W.: 1984, 'Inversion of Horizontal Loop Electromagnetic Frequency Soundings', *Geophysics* **49**, 150–164.

Garg, N. R. and Keller, G. V.: 1986, 'Spatial and Temporal Analysis of Electromagnetic Survey Data', *Geophysics* **51**, 85–89.

Goldstein, M. A. and Strangway, D. W.: 1975, 'Audio Frequency Magnetotellurics with a Grounded Electric Dipole Source', *Geophysics* **40**, 669–683.

Gómez-Treviño, E. and Edwards, R. N.: 1983, 'Electromagnetic Soundings in the Sedimentary Basin of Southern Ontario – a Case History', *Geophysics* **48**, 311–330.

Gómez-Treviño, E.: 1987a, 'Nonlinear Integral Equations for Electromagnetic Inverse Problems', *Geophysics* **52**, 1297–1302.

Gómez-Treviño, E.: 1987b, 'A Simple Sensitivity Analysis of Time-Domain and Frequency-Domain Electromagnetic Measurements', *Geophysics* **52**, 1418–1423.

Greenhouse, J. P. and Bailey, R. C.: 1981, 'A Review of Geomagnetic Variation Measurements in the Eastern United States: Implications for Continental Tectonics', *Can. J. Earth Sci.* **18**, 1268–1289.

Gunderson, B. M., Newman, G. A. and Hohmann, G. W.: 1986, 'Three-Dimensional Transient Electromagnetic Responses for a Grounded Source', *Geophysics* **51**, 2117–2130.

Gupta, P. K., Bennett, L. A. and Raiche, A. P.: 1987, 'Hybrid Calculations of the Three-Dimensional Electromagnetic Response of Buried Conductors', *Geophysics* **52**, 301–306.

Gupta, P. K., Raiche, A. P. and Sugeng, F.: 1989, 'Three-Dimensional Time-Domain Electromagnetic Modelling Using a Compact Finite-Element Frequency-Stepping Method', *Geophysical Journal* **96**, 457–468.

Heikka, J., Zhamaletdinov, A. A., Hjelt, S. E., Demidova, T. A. and Velikhov, Ye. P.: 1984, 'Preliminary Results of MHD Test Registrations in Northern Finland', *Journal of Geophysics* **55**, 199–202.

Hermance, J. F.: 1983, 'Electromagnetic Induction Studies', *Rev. Geophys.* **21**, 652–665.

Hohmann, G. W.: 1975, 'Three-Dimensional Induced Polarization and Electromagnetic Modelling', *Geophysics* **40**, 309–324.

Hördt, A.: 1989, 'Ein Verfahren zur "Joint Inversion" angewandt auf "Long Offset Transient Electromagnetics" (LOTEM) und Magnetotellurik (MT)', Diplomarbeit, Institut für Geophysick und Meteorologie der Universitat zu Köln.

Jones, A. G.: 1983a, 'On the Equivalence of the "Niblett" and "Bostick" Transformations in the Magnetotelluric Method', *Journal of Geophysics* **53**, 72–73.

Jones, A. G.: 1983b, 'The Problem of Current Channelling: A Critical Review', *Geophysical Surveys* **6**, 79–121.

Jones, A. G.: 1988, 'Static Shift of Magnetotelluric Data and its Removal in a Sedimentary Basin Environment', *Geophysics* **53**, 967–978.

Jones, A. G.: 1991, 'Electrical Conductivity of the Continental Lower Crust', in D. M. Fountain, R. J. Arculus and R. W. Kay (eds.), *Continental Lower Crust*, Elsevier.

Kaikkonen, P., Vanyan, L. L., Demidova, T. A., Yegorov, I. V. and Palshin, N. A.: 1988, 'Numerical Modelling of Deep Dipole-Dipole MHD Sounding', *Physics of the Earth and Planetary Interiors* **50**, 226–229.

Kaufman, A. A. and Keller, G. V.: 1983, 'Frequency and Transient Soundings', *Methods of Geochemistry and Geophysics*, 16, Elsevier Scientific Publishing Co., New York.

Keller, G. V., Pritchard, J. I., Jacobson, J. J. and Harthill, N.: 1984, 'Megasource Time-Domain Electromagnetic Sounding Methods', *Geophysics* **49**, 993–1009.

Kurtz, R. D., Macnae, J. C. and West, G. F.: 1989, 'A Controlled-Source, Time-Domain Electromagnetic Survey over an Upthrust Section of Archean Crust in the Kapuskasing Structural Zone', *Geophys. J. Int.* **99**, 195–203.

Lee, K. H., Pridmore, D. F. and Morrison, H. F.: 1981, 'A Hybrid Three-Dimensional Electromagnetic Modelling Scheme', *Geophysics* **46**, 796–805.

Lienert, B. R. and Bennett, D. J.: 1977, 'High Electrical Conductivities in the Lower Crust of the Northwestern Basin and Range: An Application of Inverse Theory to a Controlled-Source Deep-

Magnetic-Sounding Experiment', in J. G. Heacock (ed.), *The Earth's Crust*, AGU Monograph 20, pp. 531–552.

Lienert, B. R.: 1979, 'Crustal Electrical Conductivities Along the Eastern Flank of the Sierra Nevadas', *Geophysics* **44**, 1830–1845.

Mackie, R. L., Bennett, B. R. and Madden, T. R.: 1988, 'Long-Period Magnetotelluric Measurements near the Central California Coast: A Land-Locked View of the Conductivity Structure under the Pacific Ocean', *Geophys. J.* **95**, 181–194.

Macnae, J. C., Lamontagne, Y. and West, G. F.: 1984, 'Noise Processing Techniques for Time-Domain EM Systems', *Geophysics* **49**, 934–948.

Macnae, J. C. and Lamontagne, Y.: 1987, 'Imaging Quasi-Layered Conductive Structures by Simple Processing of Transient Electromagnetic Data', *Geophysics* **52**, 545–554.

Nabighian, M. N.: 1979, 'Quasi-Static Transient Response of a Conducting Half-Space: an Approximate Representation', *Geophysics* **44**, 1700–1705.

Nabighian, M. N. and Oristaglio, M. L.: 1984, 'On the Approximation of Finite Loop Sources by Two-Dimensional Lines Sources', *Geophysics* **49**, 1027–1029.

Nagy, Z.: 1988, 'Controlled Source Methods and Effects of Non-Uniform Source Fields', Reprint of a review paper given at the 9th EM induction Workshop in Sochi, USSR.

Nekut, A. G.: 1987, 'Direct Inversion of Time-Domain Electromagnetic Data', *Geophysics* **52**, 1431–1435.

Nekut, A., Connerney, J. E. P. and Kuckes, A. F.: 1977, 'Deep Crustal Electrical Conductivity; Evidence for Water in the Lower Crust', *Geophys. Res. Lett.* **4**, 239–242.

Nekut, A. and Spies, B. R.: 1989, 'Petroleum Exploration Using Controlled Source Electromagnetic Methods', *Proc. IEEE* **77**, 338–362.

Newman, G. A.: 1989, 'Deep Transient Electromagnetic Soundings with a Grounded Source over Near-Surface Conductors', *Geophys. Jour.* **98**, 587–601.

Newman, G. A., Hohmann, G. W. and Anderson, W. L.: 1986, 'Transient Electromagnetic Response of a Three-Dimensional Body in a Layered Earth', *Geophysics* **51**, 1608–1627.

Nicholls, E. A., Morrison, H. F. and Clarke, J.: 1988, 'Signals and Noise in Measurements of Low-Frequency Geomagnetic Fields', *J. Geophys. Res.* **93**, 13743–13754.

Oristaglio, M. L. and Hohmann, G. W.: 1984, 'Diffusion of Electromagnetic Fields in a Two-Dimensional Earth: A Finite Difference Approach', *Geophysics* **49**, 870–894.

Parker, R. L.: 1977, 'The Fréchet Derivative for the One-Dimensional Electromagnetic Induction Problem', *Geophys. J. R. astr. Soc.* **49**, 543–547.

Pridmore, D. F., Hohmann, G. W., Ward, S. H. and Sill, W. R.: 1981, 'An Investigation of Finite-Element Modelling for Electric and Electromagnetic Data in Three-Dimensions', *Geophysics* **46**, 1009–1024.

Raiche, A. P.: 1974, 'An Integral Equation Approach to 3-D Modelling', *Geophys. J. R. astr. Soc.* **36**, 363–376.

Schmucker, U.: 1970, 'Anomalies of Geomagnetic Variations in the Southwestern United States', *Bull. Scripps Inst. Oceanogr., Univ. Calif. Press* **13**.

Skokan, C. K. and Anderson, H. T.: 1991, 'Deep Long-Offset Transient Electromagnetic Surveys for Crustal Studies in the U.S.A.', *Phys. Earth and Plant. Int.* **66**, 39–50.

Spies, B. R.: 1988, 'Local Noise Prediction Filtering for Central Induction Transient Electromagnetic Sounding', *Geophysics* **53**, 1068–1079.

Spies, B. R.: 1989, 'Depth of Investigation in Electromagnetic Sounding Methods', *Geophysics* **54**, 872–888.

Spies, B. R. and Eggers, D. E.: 1986, 'The Use and Misuse of Apparent Resistivity in Electromagnetic Methods', *Geophysics* **51**, 1462–1471.

Spies, B. R. and Frischknecht, F. C.: 1991, 'Electromagnetic Sounding', in M. N. Nabighian (ed.), *Electromagnetic Methods in Applied Geophysics*, 2, Society of Exploration Geophysicists.

Sternberg, B. K.: 1979, 'Electrical Resistivity Structure of the Crust in the Southern Extension of the Canadian Shield – Layered Earth Models', *J. Geophys. Res.* **84**, 212–228.

Sternberg, B. K. and Clay, C. S.: 1977, 'Flambeau Anomaly: A High Conductivity Anomaly in the

Southern Extension of the Canadian Shield', in J. G. Heacock (ed.), *The Earth's Crust, Geophys. Monogr. Ser.*, vol 20, pp. 501–530.

Sternberg, B. K.: 1990, 'High-Accuracy, Simultaneous Calibration of Signal Measuring Systems', *Measurement Science and Technology* **1**, 225–230.

Sternberg, B. K., Washburne, J. C. and Pellerin, L.: 1988, 'Correction for Static Shift in Magnetotellurics Using Transient Electromagnetic Soundings', *Geophysics* **53**, 1459–1468.

Strack, K. M.: 1984, 'The Deep Transient Electromagnetic Sounding Technique', First field test in Australia, *Explor. Geophys.* **15**, 251–259.

Strack, K.-M., Hanstein, T. H. and Eilenz, H. N.: 1989a, 'LOTEM Data Processing in Areas with High Cultural Noise Level', *Phys. Earth and Plant. Int.* **53**, 261–269.

Strack, K.-M., Hanstein, T. H., LeBrocq, K., Moss, D. C., Vozoff, K. and Wolfgram, P. A.: 1989b, 'Case Histories of Long-Offset Transient Electromagnetics (LOTEM) in Hydrocarbon Prospective Areas', *First Break* **7**, 467–477.

Strack, K.-M., Lüschen, E. and Kotz, : 1990, 'Long-Offset Transient Electromagnetic (LOTEM) Depth Soundings Applied to Crustal Studies in the Black Forest and Swabian Alb, Federal Republic of Germany', *Geophysics* **55**, 834–842.

Towle, J. N.: 1980, 'Observations of Direct Current Concentration on the Eastern Sierran Front: Evidence for Shallow Crustal Conductors on the Eastern Sierran Front and Beneath the Coso Range', *J. Geophys. Res.* **85**, 2484–2490.

Vanyan, L. L.: 1965, 'Fundamentals of Electromagnetic Sounding', Nedra Press, Moscow (translated from Russian by G. V. Keller), 1967, in Electromagnetic Depth Soundings, Consultants Bureau, New York.

Vanyan, L. L., Demidova, T. A., Egorov, I. V. and Palshin, N. A.: 1987, 'Numerical Modelling of Deep DC-Soundings', *Geoexploration* **24**, 125–130.

Vanyan, L. L., Demidova, T. A., Palshin, N. A., Zhamaletdinov, A. A., Kuksa, Yu. I., Kaikkonen, P. and Korja, T.: 1989, 'Interpretation of Deep DC Soundings in the Baltic Shield', *Phys. Earth and Planet. Interiors* **54**, 149–155.

van Zijl, J. S. V.: 1969, 'A Deep Schlumberger Sounding to Investigate the Electrical Structures of the Crust and Upper Mantle in South Africa', *Geophysics* **34**, 450–462.

van Zijl, J.S.V., Hugo, P. L. V. and de Bellocq, J. H.: 1970, 'Ultra Deep Schlumberger Sounding and Crustal Conductivity Structure in South Africa', *Geophys. Prospect.* **18**, 615–634.

van Zijl, J. S. V. and Joubert, S. J.: 1975, 'A Crustal Model for South African Precambrian Granitic Terrains Based on Deep Schlumberger Soundings', *Geophysics* **40**, 657–663.

Varentsov, Iv. M.: 1983, 'Modern Trends in the Solution of Forward and Inverse 3D Electromagnetic Induction Problems', *Geophysical Surveys* **6**, 55–78.

Vasseur, G. and Weidelt, P.: 1977, 'Bimodal Electromagnetic Induction in Non-Uniform Thin Sheets with an Application to the Northern Pyrenean Induction Anomaly', *Geophys. J. Roy. astr. Soc.* **51**, 669–690.

Velikhov, Ye. P., Zhamaletdinov, A. A., Belkov, I. V., Gorbunov, G. I., Hjelt, S. E., Lisin, A. S., Vanyan, L. L., Zhdanov, M. S., Demidova, T. A., Korja, T., Kirillov, S. K., Kuksa, Yu. I., Poltanov, A. Ye., Tokarev, A. D. and Yevstigneyev, V. V.: 1986, 'Electromagnetic Studies on the Kola Peninsula and in Northern Finland by Means of a Powerful Controlled Source', *Journal of Geodynamics* **5**, 237–256.

Vozoff, K. and Jupp, D. L. B.: 1975, 'Joint Inversion of Geophysical Data', *Geophys. J. R. astr. Soc.* **42**, 977–991.

Vozoff, K., Moss, D., LeBrocq, K. L. and McAllister, K.: 1985, 'LOTEM Electric Field Measurements for Mapping Resistive Horizons in Petroleum Exploration', *Bull. Soc. Austral. Explor. Geophys.* **16**, 309–311.

Wait, J. R.: 1982, *Geoelectromagnetism*, Academic Press, New York, 268 pp.

Wannamaker, P. E.: 1983, 'Resistivity Structure of the Northern Basin and Range', *Geothermal Resources Council Special Report* **13**, 345–362.

Ward, S. H.: 1983, 'Controlled Source Electrical Methods for Deep Exploration', *Geophysical Surveys* **6**, 137–152.

Ward, S. H. and Hohmann, G. W.: 1988, 'Electromagnetic Theory for Geophysical Applications', in M. N. Nabighian (ed.), *Electromagnetic Methods in Applied Geophysics*, Vol 1, pp. 131–312, SEG, Tulsa.

Weidelt, P.: 1975, 'Electromagnetic Induction in 3D Structures', *J. Geophys.* **41**, 85–109.

West, G. F., Macnae, J. C. and Lamontagne, Y.: 1984, 'A Time-Domain EM System Measuring the Step Response of the Ground', *Geophysics* **49**, 1010–1026.

West, G. F. and Edwards, R. N.: 1985, 'A Simple Parametric Model for the Electromagnetic Response of an Anomalous Body in a Host Medium', *Geophysics* **50**, 2542–2557.

Wilhelm, H., Berktold, A., Bonjer, K.-P., Jäger, K., Stiefel, A. and Strack, K.-M.: 1989, 'Heat Flow, Electrical Conductivity and Seismicity in the Black Forest Crust, SW Germany', in R. F. Mereu, S. Mueller and D. M. Fountain (eds.), *Properties and Processes of Earth's Lower Crust*, Amer. Geophys. Union, Geophys. Monogr. 215–232.

Wilt, M. J., Goldstein, N. E., Stark, M., Haught, J. R. and Morrison, H. F.: 1983, 'Experience with the EM-60 Electromagnetic System for Geothermal Exploration in Nevada', *Geophysics* **48**, 1090–1101.

Wilt, M. J., Morrison, H. F., Lee, K. H. and Goldstein, N. E.: 1989, 'Electromagnetic Sounding in the Columbia Basin, Yakima, Washington', *Geophysics* **54**, 952–961.

Woods, D. V. and Allard, M.: 1986, 'Reconnaissance Electromagnetic Induction Study of the Kapuskasing Structural Zone: Implications for Lower Crustal Conductivity', *Phys. Earth Planet. Int.* **42**, 135–142.